UNIVERSITY OF TWENTE.

Master Thesis

Modeling,Design and characterization of a thermal flow sensor

Yi Wang,BSc
Supervisors
dr.ir.R.J.WIEGERINK
dr.ir.J.GROENESTEIJN

Faculty of Electrical Engineering,
Mathematics and Computer Science
Integrated Devices and Systems

University of Twente
P.O. Box 217
7500 AE Enschede
The Netherlands

Abstract

In this thesis, a new analytical model is introduced to predict the performance of a thermal flow sensor. The analytical model is based on the heat equations, and we add the heat-sink item into the equation, to ensure the calculation result is closer to the real performance. To verify the model, we also built a Comsol model, and the temperature profile of the analytical model is near agreement with Comsol model. Furthermore, the result of the analytical model also compares to the measuring result of the thermal flow sensor which provides by Bronkhorst.

Contents

Nomenclature

Symbol List

α	Temperature coefficient	$1/K$
A	area	um^2
c_p	Heat capacity at constant pressure	$kJ/(kgK)$
G	Heat sink's thermal conductivity	$K/(Wm)$
H_{flat}	Height of the flat structure	nm
H_{heater}	Thickness of heater	nm
k	Thermal conductivity	$W/(m^{-1}K^{-1})$
k_{eff}	Effective thermal conductivity	$W/(m^{-1}K^{-1})$
L	Length of beam	m
L_{gap}	Gap between heaters	um
L_{heater}	Length of heater	um
ρ	Density	$kg/(m^3)$
P	Power	mW
Q	Heat flux density	W/m^{-3}
R	Resistance of heater	Ω
$R1$	Radius of channel	um
$R2$	Distance between center of channel and heat sink	um
T	Temperature	$^{\circ}C$
t	Time	s

$t_{channel}$	Thickness of of channel wall	um
V	Potential	V
v	Velocity	m/s
$W_{channel}$	Diameter of the channel	um
W_{flat}	Width of the flat structure	um
W_{heater}	Width of heater	um
x	Position of beam	m

Chapter 1

Introduction

1.1 Background and motivation

Nowadays, the thermal flow sensor is widely used in many areas, such as a drug delivery system, chemical analysis, printer, etc.. As those industries developed, the people have higher requirements for the thermal flow sensor, such as higher sensitivity, larger measurement range, and lower pressure drop. To design such a suitable sensor, we need to have an idea about how the parameters can influence the performance of the sensor. Thus we need to create a model to construct the thermal flow sensor. Usually, the researcher would like to use an FEA(finite element analysis) software to make a thermal flow sensor model, such as Comsol [1] and ANSYS [2], the software can provide an accurate prediction of a thermal flow sensor, but the time consumption is high. Thus, in this thesis, we will introduce a new analytical model to construct the thermal flow sensor. The figure 1.1 shows the schematic of the actual sensor. The fluid will go through the closed channel via the inlet which placed in the backside of the channel, then the temperature distribution of the heater will be changed by applying the flow. Meanwhile, the resistance value of the heater embedded on the top of the channel will change, by measuring the resistance difference, we can derive the velocity of flow.

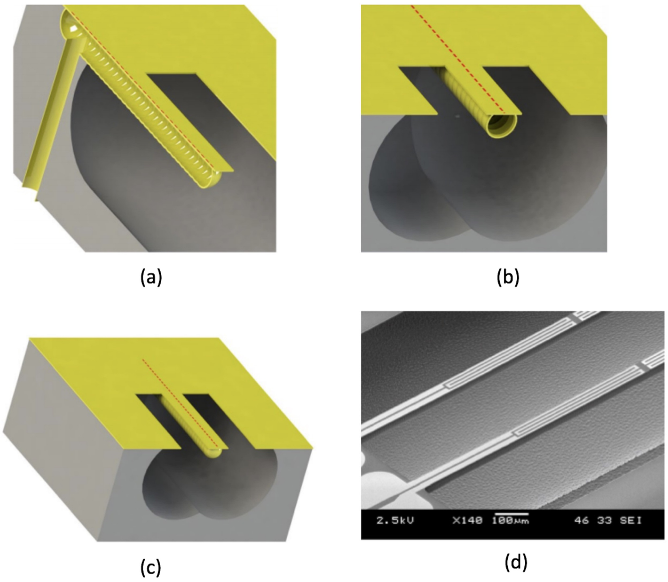

Figure 1.1: The schematic of the actual sensor. $\boldsymbol{a}$**.** Artist impressions of inlet of the sensor. $\boldsymbol{b}$**.** Artist impressions of channel of the sensor. $\boldsymbol{c}$**.** Artist impressions of the sensor. $\boldsymbol{d}$**.** SEM picture of the heater.Picture takes from [3]

1.2 Thesis Outline

Chapter 2 describes two models for the thermal flow sensor. An analytical model can be used to plot the temperature profile of the sensor in the flow direction. Later, a finite element model in Comsol is also presented to verify the analytical model/

Chapter 3 will present the measurement results of actual sensors which provide by Bronkhorst [4]. The measurement results will be used to compare with the analytical simulation results to see how close they are. Later on, we will change some parameters, such as the distance between the two heaters, the channel's length, etc., to get an understanding of those parameters to influence the sensor.

Chapter 2

Theory and Modeling of thermal flow sensors

To understand the physics of the thermal flow sensor. This chapter will start by introducing the basic heat equation. Then based on the heat equation, the analytical model will be made to construct the thermal flow sensor. Also, a finite element model in Comsol will be built to verify the analytical model. Next, to make the analytical model more flexible, we will add more heaters in the analytical model. Again, a corresponding finite element model will be built to verify the results. Furthermore, based on the analytical model we made, the heat-sink will be added in the analytical model to understand how the heat-sink influence the behavior of the thermal flow sensor.

2.1 Thermal Equation

To derive the temperature profile of the thermal flow sensor, we start from the general heat equation [5]:

$$\rho c_p[\frac{\partial T}{\partial t} + (\overrightarrow{v} \cdot \nabla)T] = k \cdot T\nabla^2 + Q \tag{2.1}$$

With ρ is the fluid's density, c_p is the heat capacity at constant pressure,T is the temperature, t is the time,v is the velocity, k is thermal conductivity and Q is heat source(density).

Firstly, we assume there is no flow through the channel, and the temperature does not depend on the time, then the equation reduces to:

$$0 = k \cdot T\nabla^2 + Q \tag{2.2}$$

Since we only interesting the temperature profile in the flow direction, see figure

2.1. Then the heat equation reduces to:

$$0 = k\frac{d^2T}{dx^2} + Q \tag{2.3}$$

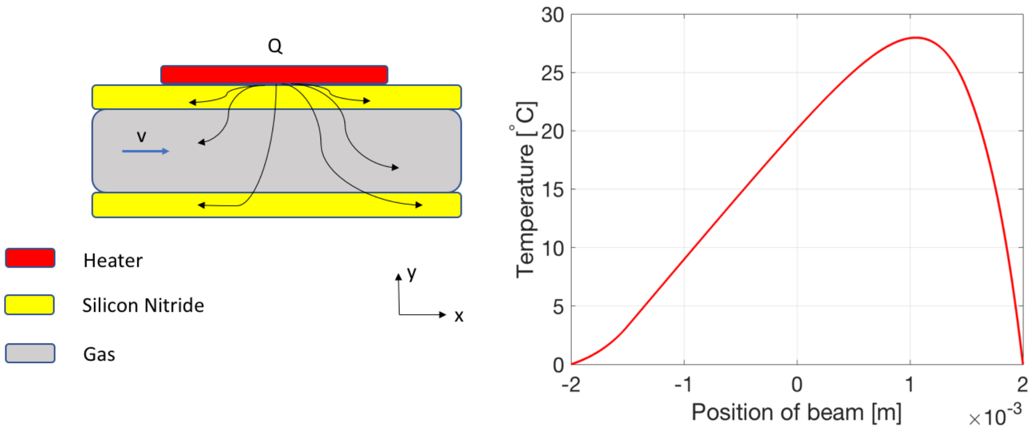

Figure 2.1: Illustration of the how the temperature changes as applying flow. The heater placed in the middle generates the heat flow Q(donated by black arrows), and the heat flow will go through the fluid and silicon nitride. As applying the flow, the heat flux in the downstream will be larger the heat flux in the upstream. This will result in the temperature at downstream higher than the temperature upstream.

To construct the model, we need to define the geometry and boundary condition. The figure 2.2 shows the sketch of the one-dimensional model. There are is one heater in the middle, and At $x = \pm L$ the temperature will be assumed as room temperature.According to the figure 2.2, the equation 2.3 can be divided into two equations:

$$0 = k\frac{d^2T}{dx^2} + Q \quad if|x| \leq x_h \tag{2.4}$$

$$0 = k\frac{d^2T}{dx^2} \quad if \quad else \tag{2.5}$$

Then the temperature at flow direction can be calculated as :

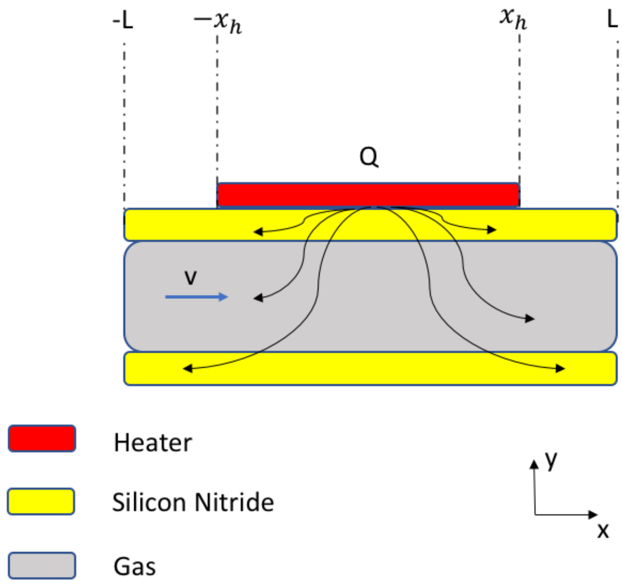

Figure 2.2: The structure of the one-dimensional model. The heater with length $2x_h$ dissipates Q watts per cubic meter. At $x = \pm L$ the silicon acts as the heatsink which at room temperature.

$$T(x) = \begin{cases} A_1 x + B_1, & \text{for} -L \le x \le -x_h \quad (2.6) \\ \frac{-Qx^2}{2k} + Cx + D, & \text{for} |x| \le -x_h \quad (2.7) \\ A_2 x + B_2, & \text{for} x_h \le x \le L \quad (2.8) \end{cases}$$

With $2L$ is the tube length and $2x_h$ is the heater length.

To solve the equation 2.6-2.8, we need to find six equations from the boundary conditions. Firstly, at $x = \pm L$ the beam at room temperature, then it can be assumed that:

$$T(-L) = T(L) = T_{room} \tag{2.9}$$

secondly, the temperature should be continuous at $x = \pm x_h$:

$$T_{left}(-x_h) = T_{heater}(-x_h) \tag{2.10}$$

$$T_{right}(x_h) = T_{heater}(x_h) \tag{2.11}$$

The heat flux should also be continuous at $x = \pm x_h$:

$$[k\frac{dT_{left}}{dx}]_{x=-x_h} = [k\frac{dT_{heater}}{dx}]_{x=-x_h} \tag{2.12}$$

$$[k\frac{dT_{right}}{dx}]_{x=x_h} = [k\frac{dT_{heater}}{dx}]_{x=x_h} \tag{2.13}$$

By applying those boundary conditions into the equation 2.6-2.8, then we can get 6 equations, by solving those equations we can obtain the values for A_1, B_1,C,D,A_2 and B_2::

$$A_1 = -A_2 = \frac{Qx_h}{k} \tag{2.14}$$

$$C = 0 \tag{2.15}$$

$$D = \frac{Qx_h(L - \frac{x_h}{2})}{k} + T_{heatsink} \tag{2.16}$$

$$B_1 = B_2 = T_{heatsink} + \frac{Qx_nL}{k} \tag{2.17}$$

If we include the velocity into the equation, the differential equation becomes:

$$0 = k\frac{d^2T}{dx^2} - \rho c_p v\frac{dT}{dx} + Q \quad if|x| \le x_h \tag{2.18}$$

$$0 = k\frac{d^2T}{dx^2} - \rho c_p v\frac{dT}{dx} \quad if \quad else \tag{2.19}$$

Then the temperature at flow direction can be calculated as :

$$T(x) = \begin{cases} A_1 e^{\frac{\rho c_p v x}{k}} + B_1, & \text{for } -L \leq x \leq -x_h \quad (2.20) \\ C_1 e^{\frac{\rho c_p v x}{k}} + C_2 + \dfrac{Qx}{\rho c_p v}, & \text{for} |x| \leq -x_h \quad (2.21) \\ A_2 e^{\frac{\rho c_p v x}{k}} + B_2, & \text{for} x_h \leq x \leq L \quad (2.22) \end{cases}$$

Substituting $r = \frac{\rho c_p v}{k}$, and applying same boundary conditions as previously, then we have six equations as following:

$$A_1 e^{-rL} + B_1 = T_{room}, x = -L \tag{2.23}$$

$$A_2 e^{rL} + B_2 = T_{room}, x = L \tag{2.24}$$

$$A_1 e^{-rx_h} + B_1 = C_1 e^{-rx_h} + C_2 - \frac{Qx_h}{rk}, x = -x_h \tag{2.25}$$

$$A_2 e^{rx_h} + B_2 = C_1 e^{rx_h} + C_2 + \frac{Qx_h}{rk}, x = x_h \tag{2.26}$$

$$A_1 r e^{-rx_h} = C_1 r e^{-rx_h} + \frac{Q}{rk}, x = -x_h \tag{2.27}$$

$$A_2 r e^{rx_h} = C_1 r e^{rx_h} + \frac{Q}{rk}, x = x_h \tag{2.28}$$

The equation 2.23 and 2.24 describe the temperature at the edges of the channel which $x = \pm L$, the equation 2.25 and 2.26 describe the temperature is continuous at $x = \pm x_h$, the last two equations decribes the heat flux at $x = \pm x_h$ is also continuous. The detail about how to solve these constant can be found in appendix A, then the constant can be calculated as:

$$A_1 = \frac{Q(e^{r(L+x_h)} - e^{r(L-x_h)} - 2x_h r)}{r^2 k(e^{rL} - e^{-rL})} \tag{2.29}$$

$$A_2 = \frac{Q(e^{-r(L-x_h)} - e^{-r(L+x_h)} - 2x_h r)}{r^2 k(e^{rL} - e^{-rL})} \tag{2.30}$$

$$B_1 = -e^{-rL} Q(\frac{(e^{r(L+x_h)} - e^{r(L-x_h)} - 2x_h r)}{r^2 k(e^{rL} - e^{-rL})}) \tag{2.31}$$

$$B_2 = -e^{rL}Q(\frac{(e^{-r(L-x_h)} - e^{-r(L+x_h)} - 2x_h r)}{r^2k(e^{rL} - e^{-rL})}) \tag{2.32}$$

$$C_1 = Q(\frac{(e^{-r(L-x_h)} - e^{r(L-x_h)} - 2x_h r)}{r^2k(e^{rL} - e^{-rL})}) \tag{2.33}$$

$$C_2 = Q(\frac{((rx_h + 1)e^{rL} - (rx_h + 1)e^{-rL} - e^{rx_h} + e^{-rx_h} + 2x_h re^{-rL})}{r^2k(e^{rL} - e^{-rL})}) \tag{2.34}$$

To construct the analytical model, we need to define the simulation parameters. The figure 2.3 provide the schematic overview of the parameters of the channel, and the table 2.1 gives the value for those parameters.

Parameters	Value	Unit	Symbol
Thickness of the heater	200	nm	H_{heater}
Width of the heater	100	um	W_{heater}
Length of the heater	3000	um	$2 * L_{heater}$
Diameter of the channel	63	um	$W_{channel}$
Channel wall thickness	1	um	$t_{channel}$
Width of flat structure	100	um	W_{flat}
Height of flat structure	3.7	um	H_{flat}
Channel length	2000	um	L
density of Nitrogen	1000	kgm^{-3}	ρ
Heat power	1	mW	P
Conductivity of gold	314	W/mK	k_{gold}
Conductivity of SiRN	20	W/mK	k_{SiRN}
Conductivity of Nitrogen	26e-3	W/mK	k_{SiRN}

Table 2.1: The simulation parameters for analytical model

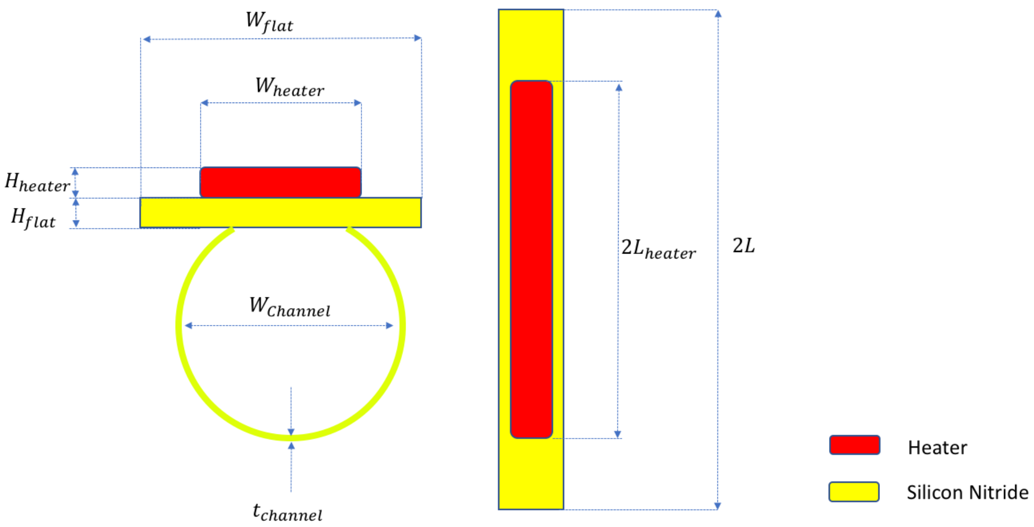

Figure 2.3: The schematic overview of the channel.Right: the cross section of the channel. Left : the top view of the channel.

Because the analytical model is in the one-dimensional equation, then we need to calculate the effective conductivity k_{eff} of the sensor:

$$k_{eff} = \frac{k_{gold}A_{heater} + k_{SiRN}A_{SiRN} + k_{Nitrogen}A_{channel}}{A_{total}} \tag{2.35}$$

In which A is the cross sectional area.

In the equation 2.20, we use Q to indicate the heater source, but in the table 2.1, the heater source is P. Thus we need to divide the entire volume of the tube to calculate the heat density Q which is $0.1433e9[Wm^{-3}]$.

By filling the data from the table 2.1 into equation 2.20, the relation between the velocity of flow and temperature can be described in figure 2.4.

From the figure 2.4 it can be seen that as the flow increases, the temperature distribution will move in the same direction as flow.

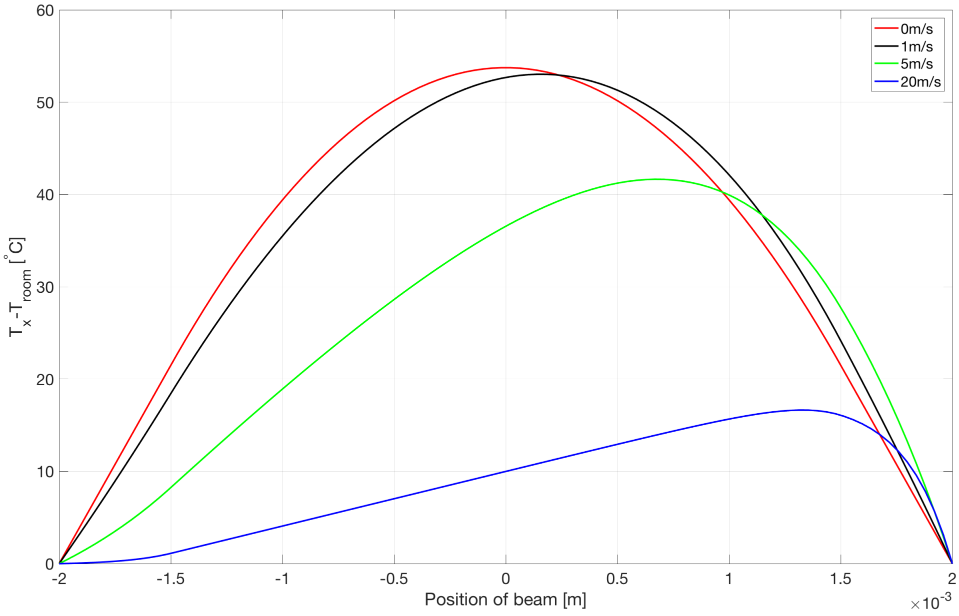

Figure 2.4: The relation between velocity and temperature. As the flow increases, the temperature profile will shift as same direction as flow.

2.2 Numerical simulations

In this section, the finite element model will be made in COMSOL Multiphysics 5.3 to verify the analytical model. The figure 2.7 shows the overview schematic of the simulation model.

At the inlet and outlet, the temperature is fixed to the room temperature. The heater is replaced in the middle of the channel which can generate the 1 mW power. To make the Comsol model is comparable with the analytical model, we will use the same parameter as table 2.1.

The figure 2.8 shows the COMSOL simulation result. As applying the flow, the temperature profile shift in the same direction as flow. To compare both simulations quantitatively, we will subtract the temperature of both simulations and then divide by the maximum temperature to calculate the relative average temperature difference, see equation 2.36. For the $v = 0m/s$, there is 12% relative average temperature difference between two simulations. For the $v = 1m/s$, the relative average temperature difference is 16%. For the $v = 5m/s$, the relative average temperature difference different is 9.5% and the relative average temperature difference at $v = 20m/s$ is 8%. The reason behind it is because the geometrical detail is not taken into consideration in the Matlab model. Thus the effective conductivity

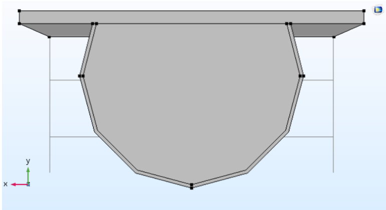

Figure 2.5: Cross Section of Channel

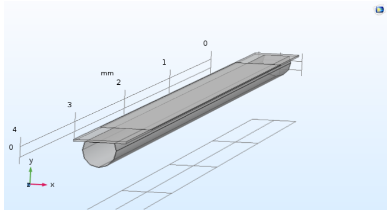

Figure 2.6: Side View of Channel

Figure 2.7: Overview of the simulation schematic.Left: cross section of the tube. Right: side view of the tube

in Matlab will have some difference compare to Comsol simulation.

$$\sigma_{temperature} = \frac{\sum_{k=1}^{k=n} (T_{Comsol} - T_{analytical})}{T_{maximum} * n} \tag{2.36}$$

In which $\sigma_{temperature}$ is relative average temperature difference, n is simulation mesh points and $T_{maximum}$ is maximum temperature of Comsol simulation.

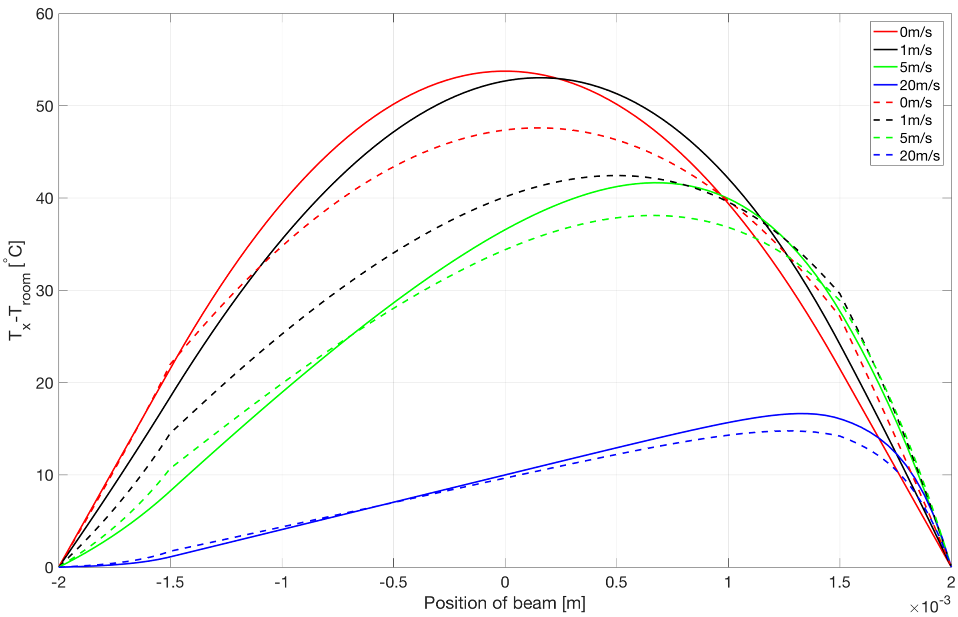

Figure 2.8: The comparison between COMSOL and Matlab simulation result, the solid line indicates the result from the Matlab and the dash line indicates the result from COMSOL

2.3 Thermal Equation with Different Geometry

To make the analytical model more flexible, in this section, more heaters will be added to the analytical model. Then the analytical model can provide the simulation results for the sensor up to 3 heaters.

To include the more heaters in the model, we need to recall the heat equation 2.1. The figure2.9 shows the new schematic of thermal flow sensor. Compare to the previous schematic, and there are three heaters placed on the channel, then we can change the value of Q and $Q1$ to determine the number of heaters. At the $Q = 0$, it means the sensor includes two heaters, and we even can choose the different heat flux density for these two heaters. At the $Q1 = 0$, there is only one heater in the sensor. If we want to simulate the sensor with three heaters, then we can set the Q and $Q1$ to the value we want.

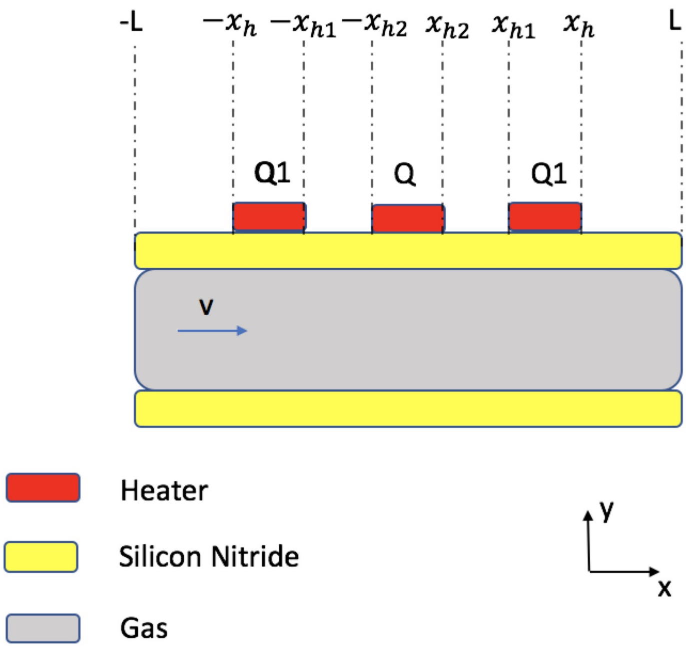

Figure 2.9: The new geometry of thermal sensor. There are three heater place on the sensor, by changing the Q, we can simulation the model in the different cases

The equation becomes more complicated because of two more heaters is added:

$$T(x) = \begin{cases} A_1 e^{\frac{\rho c_p v x}{k}} + B_1, & \text{for} -L \leq x \leq -x_h & (2.37) \\ C_1 e^{\frac{\rho c_p v x}{k}} + C_2 + \dfrac{Q1x}{\rho c_p v}, & \text{for} -x_h \leq x \leq -x_{h1} & (2.38) \\ A_2 e^{\frac{\rho c_p v x}{k}} + B_2, & \text{for} -x_{h1} \leq x \leq -x_{h2} & (2.39) \\ C_3 e^{\frac{\rho c_p v x}{k}} + C_4 + \dfrac{Qx}{\rho c_p v}, & \text{for} -x_{h2} \leq x \leq x_{h2} & (2.40) \\ A_3 e^{\frac{\rho c_p v x}{k}} + B_3, & \text{for} x_{h2} \leq x \leq x_{h1} & (2.41) \\ C_5 e^{\frac{\rho c_p v x}{k}} + C_6 + \dfrac{Q1x}{\rho c_p v}, & \text{for} x_{h1} \leq x \leq x_h & (2.42) \\ A_4 e^{\frac{\rho c_p v x}{k}} + B_4, & \text{for} x_h \leq x \leq L & (2.43) \end{cases}$$

Where L, x_h, x_{h1}, x_{h2} is indicated in the figure 2.9, Q1 and Q is the heat flux density of heater.

The similar boundary condition as section 2.1 will be used. Firstly, at $x = \pm L$, the temperature of the equation is the same as room temperature. At $x = \pm x_h, x = \pm x_{h1}, x = \pm x_{h2}$, the temperature and heat flux is continuous . Then we can find 14 equations with 14 variables. Because these equations are too difficult to solve, these equations are solved with Wolfram Mathematica 11.1 [6]. All constants can be found in Appendix B. To verify whether the solution is correct, we assume there is only one heater in the middle, which gives the same solution as section 1 and the figure 2.10 shows the plot of two calculations.

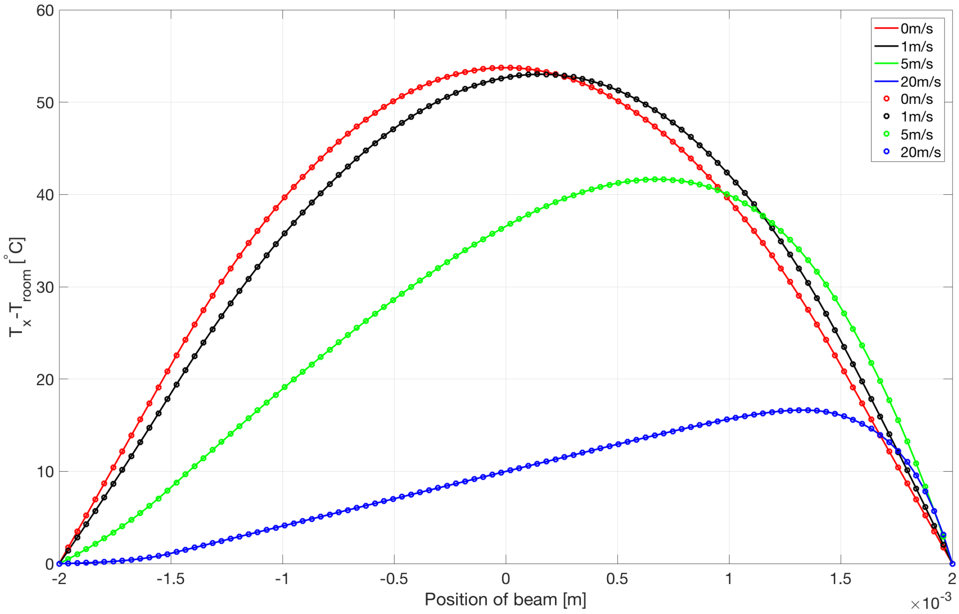

Figure 2.10: The solid line indicate the plot of equation 2.37, and the circle is the plot of equation 2.20. Under the same conditions, the two equations can get the same result.

Compared to the previous mathematical model. The new analytical model should be able to simulate the thermal flow sensor with up to three heaters. In the following section, we will run the analytical simulations for the sensor with a different structure. Again, the Comsol simulations will be used to verify the result.

2.3.1 A sensor with two heaters and large gap

Firstly, A sensor with two heaters and a large distance between heaters will be simulated. The simulation will be base on the parameters in table 2.1, in the Table 2.2 only shows the simulation parameter which is different from table 2.1. Figure 2.11 shows the overview schematic of the sensor. The figure 2.12 show the simulation result from Comsol and Matlab. At $v = 0m/s$,$v = 1m/s$,$v = 5m/s$ and $v = 20m/s$, the relative average temperature difference is 7% ,7.5%,7.38% and 7.52%. The main reason cause this difference is the analytical model doesn't consider the geometrical details of channel.

Parameters	Value	Unit	Symbol
Heater length	1000	um	L_{heater}
Gap between two heaters	1000	um	L_{gap}

Table 2.2: The new parameters for two heaters and large gap

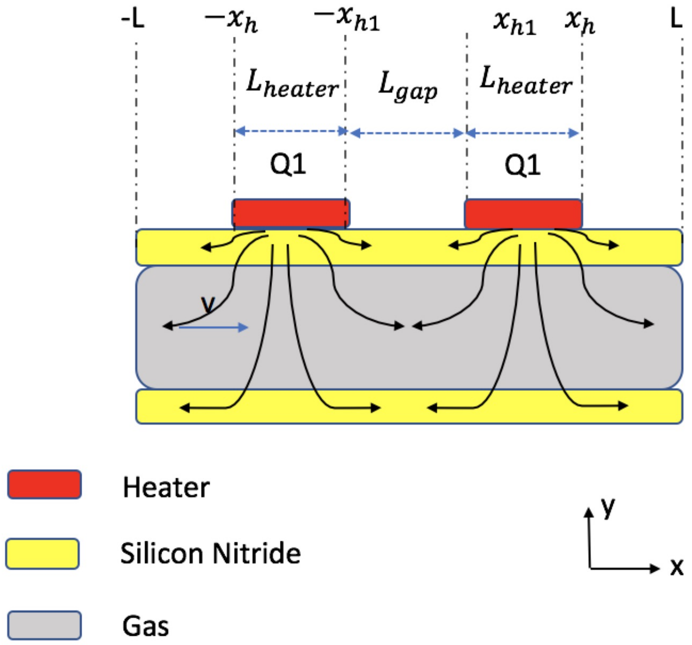

Figure 2.11: The sensor with two heaters and large distance. The two heaters will generate the same power, and dimension of two heaters is same as well

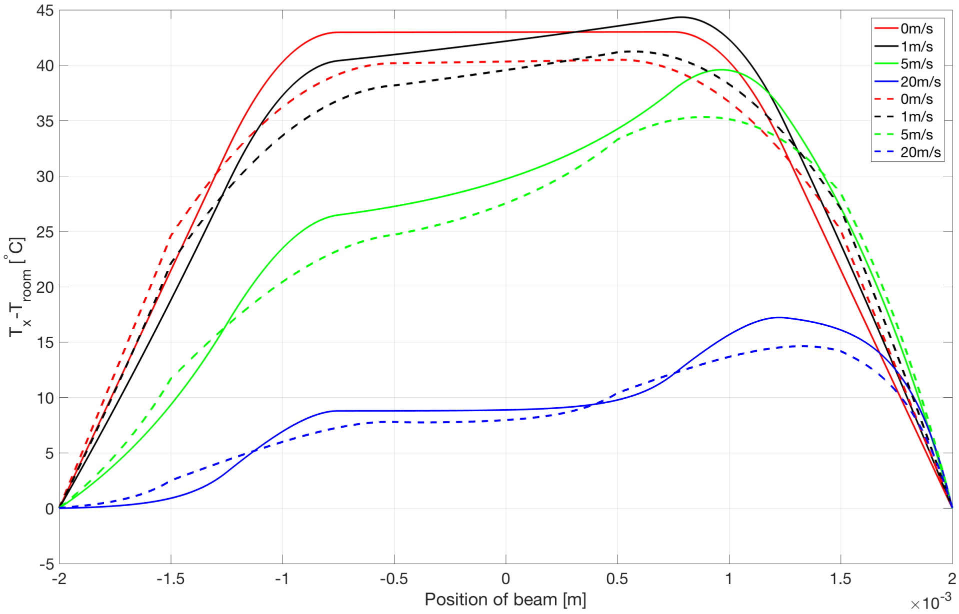

Figure 2.12: The simulation result of the sensor, the dash line indicates the simulation result whereas the solid ones indicates the analytical model. Because there is no heater between $x = -500um$ and $x = 500um$,The temperature remains same at $v = 0m/s$. As applying the flow, the maximum temperature will shift as same direction as flow.

2.3.2 The sensor with one heater in the middle

In this part, the sensor with one heater will be presented. The table 2.3 and figure 2.13 shows the changing parameters of the sensor and an overview schematic of the sensor. The figure 2.14 shows the simulation results, from the figure it can be seen that Comsol simulations gives the almost the same results as the analysis model. Compare to the figure 2.12, the temperature amplitude of one heater design is higher. It can be concluded that as the heater become shorter, the heat flux density will increase.

Parameters	Value	Unit	Symbol
Heater length	1000	um	L_{heater}

Table 2.3: The changing simulation parameters for The sensor with one heater

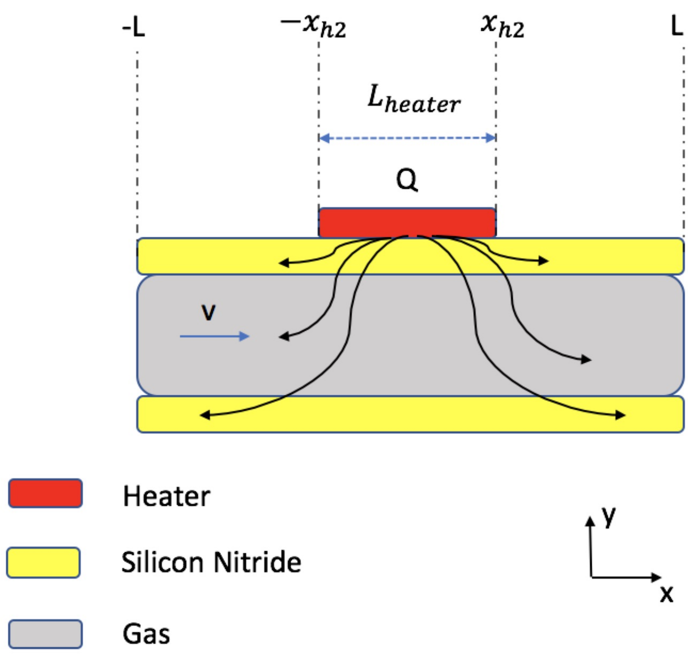

Figure 2.13: The sensor with one short heater place on the middle

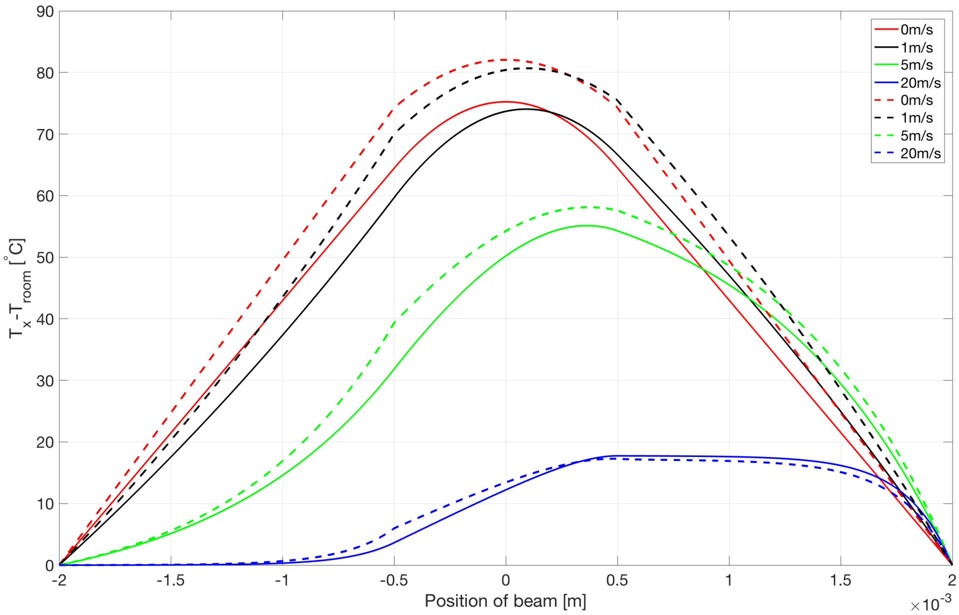

Figure 2.14: The simulation result of the sensor with one heater in the middle, the dash line indicates the simulation result whereas the solid ones indicates the analytical model. At $v = 0m/s$,$v = 1m/s$,$v = 5m/s$ and $v = 20m/s$, the relative average temperature difference is 5%,5%,5.32% and 6.5%

2.3.3 The sensor with more heaters and different heat power

In this section,more complex structures will be presented to see whether the analysis model can predict the temperature profile of the sensor. The table 2.4 and figure 2.15 shows the detail of the sensor. The figure 2.16 shows the simulation results, compared to the previous geometry, the simulation results doesn't fit with the analysis model, and the relative average temperature difference is bigger than the previous two geometries. As the geometry of the sensor becomes more complex, the difference between the calculated effective thermal conductivity and thermal conductivity in Comsol is larger.

Parameters	Value	Unit	Symbol
Heater length	500	um	L_{heater}
Distance between heaters	500	um	L_{gap}
Heat power for the middle heater	1	mW	P
Heat power for side heaters	0.5	mW	P1

Table 2.4: The new parameters for the sensor with three heaters

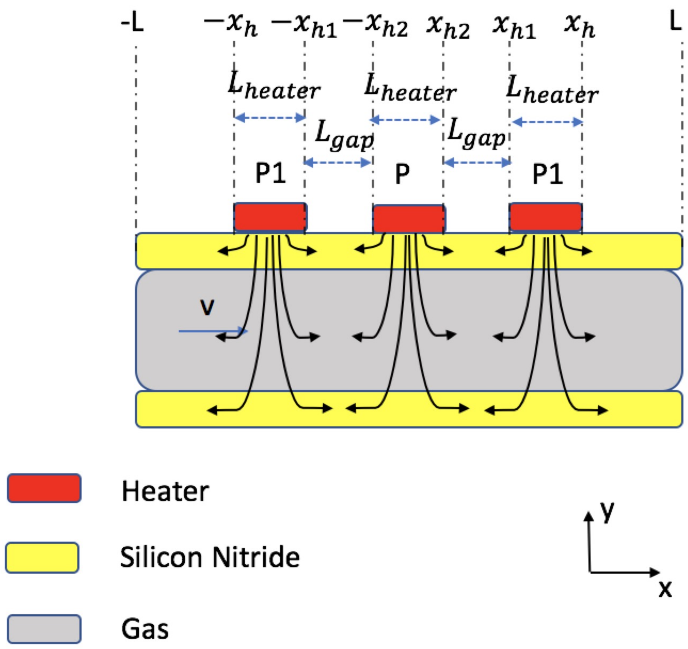

Figure 2.15: The sensor with three heaters. The heater in the middle can generated $1mW$ power, the heat between $\pm x_h$ and $\pm x_{h1}$ can generate $0.5mW$ power.

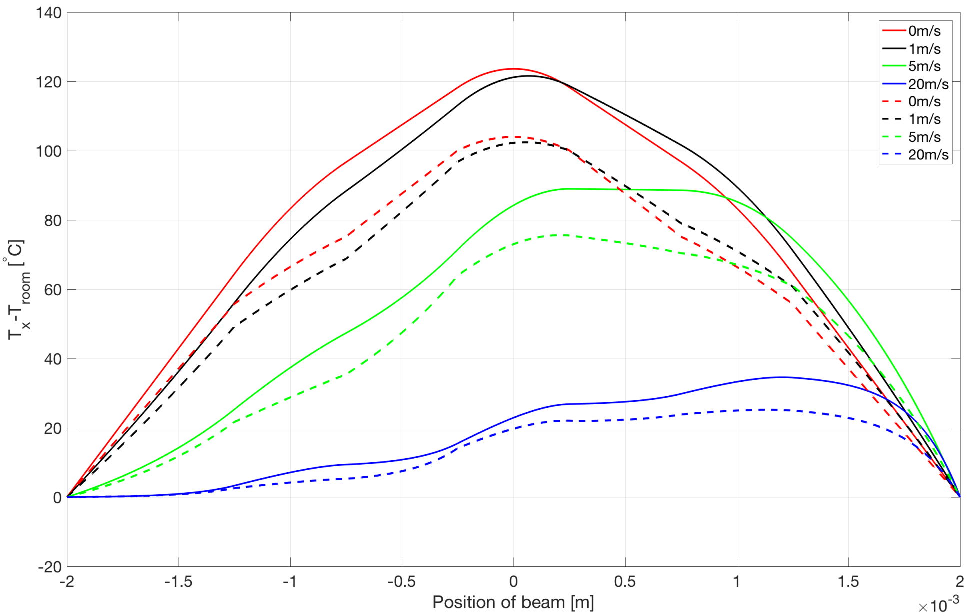

Figure 2.16: The simulation result of the sensor with Three heater in the middle, the dash line indicates the simulation result and the solid ones indicates the analytical model.At $v = 0m/s$,$v = 1m/s$,$v = 5m/s$ and $v = 20m/s$, the relative average temperature difference is 17%,20%,17% and 17%

2.4 The Sensor with Heat-sink

If we include the heat-sink, the differential heat equation becomes more complicated. Compare to the previous heat equation 2.1, and the new equation will consist of the conductivity of the heat-sink. Thus the equation can be written as:

$$0 = A_{cross}k\frac{d^2T}{dx^2} - A_{cross}\rho C_p v\frac{dT}{dx} - GT + Q' \tag{2.44}$$

With A_{cross} is area of the channel's cross section, G is the thermal line conductance of the heat-sink in $[W/(Km)]$ and Q' is line power in $[W/(m)]$. By substituting $G' = \frac{G}{A_{cross}}$:

$$0 = k\frac{d^2T}{dx^2} - \rho C_p v\frac{dT}{dx} - G'T + Q \tag{2.45}$$

Now, the temperature profile does not only depend on the flow and beam but also rely on the heat sink, see figure 2.17.

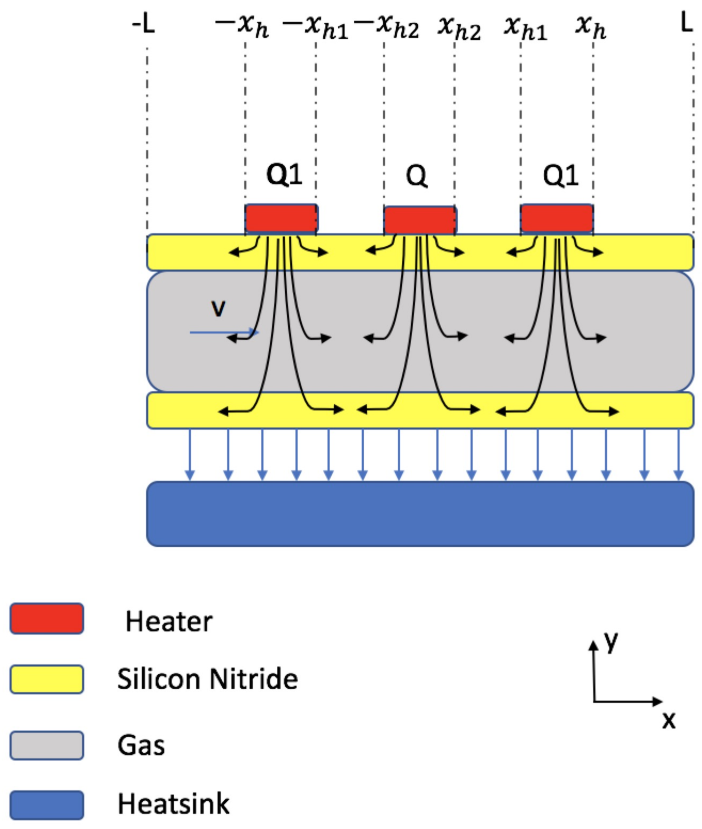

Figure 2.17: The overview schematic of the thermal flow sensor with heat-sink. The blue part indicates the heat-sink which is under the channel.

Because there is an additional item in the equation, the equation is different compared to the previous solution:

$$T(x) = \begin{cases} A_1 e^{r_1 x} + B_1 e^{r_2 x}, & \text{for} -L \leq x \leq -x_h \quad (2.46) \\ C_1 e^{r_1 x} + C_2 e^{r_2 x} + \dfrac{Q1}{G'}, & \text{for} -x_h \leq x \leq -x_{h1} \quad (2.47) \\ A_2 e^{r_1 x} + B_2 e^{r_2 x}, & \text{for} -x_{h1} \leq x \leq -x_{h2} \quad (2.48) \\ C_3 e^{r_1 x} + C_4 e^{r_2 x} + \dfrac{Q}{G'}, & \text{for} -x_{h2} \leq x \leq x_{h2} \quad (2.49) \\ A_3 e^{r_1 x} + B_3 e^{r_2 x}, & \text{for} x_{h2} \leq x \leq x_{h1} \quad (2.50) \\ C_5 e^{r_1 x} + C_6 e^{r_2 x} + \dfrac{Q1}{G'}, & \text{for} x_{h1} \leq x \leq x_h \quad (2.51) \\ A_4 e^{r_1 x} + B_4 e^{r_2 x}, & \text{for} x_h \leq x \leq L \quad (2.52) \end{cases}$$

Where L ,x_h,x_{h1} and x_{h2} are indicated in the figure 2.9,r_1 and r_2 are the two solutions of general solution which can be desirable as:

$$r_1 = \frac{\frac{\rho c_p v}{k} + \sqrt{\frac{(\rho c_p v)^2}{k^2} + \frac{4G'}{k}}}{2} \tag{2.53}$$

$$r_2 = \frac{\frac{\rho c_p v}{k} - \sqrt{\frac{(\rho c_p v)^2}{k^2} + \frac{4G'}{k}}}{2} \tag{2.54}$$

By applying the same boundary condition as previously,14 equations can be found. The solutions can be found in Appendix C.

Next, because the heat-sink is included. Then heat transfer via conduction through the air to the heat sink can be approximated by taking a cylinder [7], see figure 2.18.

$$G' = \frac{2 * \pi * k_{air}}{ln(\frac{R2}{R1}) * A_{cross}} \tag{2.55}$$

With $R1$ and $R2$ is the radius of channel and gap between the channel and heat sink, k_{air} is the thermal conductivity of air which is $26e^{-3}W/(Km)$, and A_{cross} is the cross section of channel . Then the value of G can be approximated as $2.8e^{-7}W/(Km^3)$.

Again, the Comsol model will be used to verify the analytical model,see figure 2.19.. The simulation parameters is same as table 2.2, 2.3, 2.4.

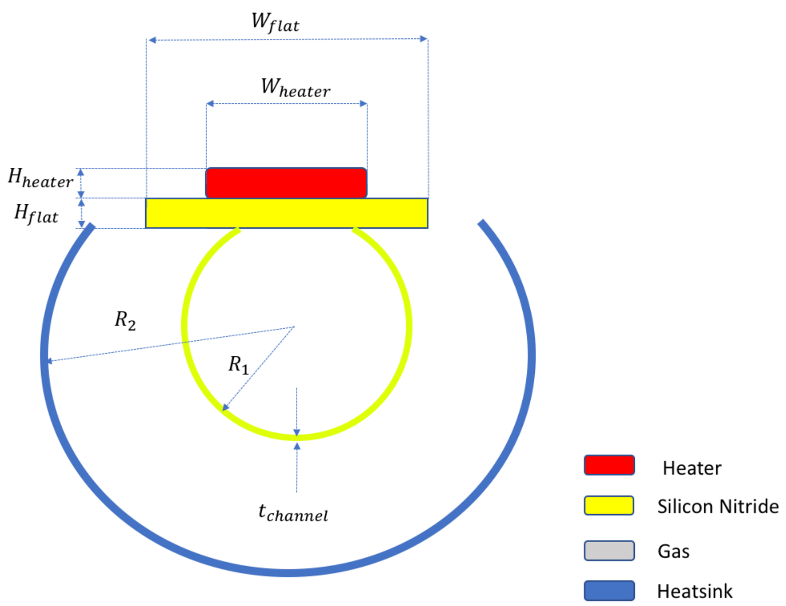

Figure 2.18: Method of Images for cylinder approximation

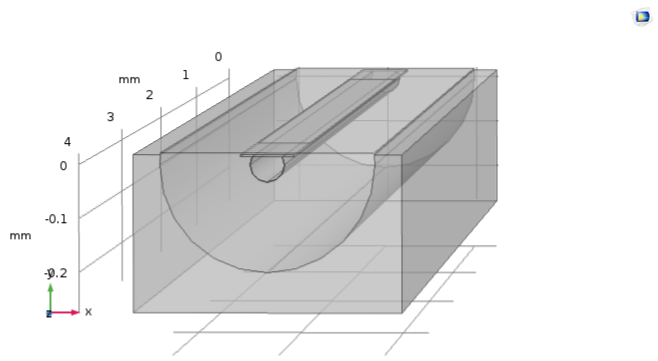

Figure 2.19: The simulation model in Comsol, which have silicon bulk layer

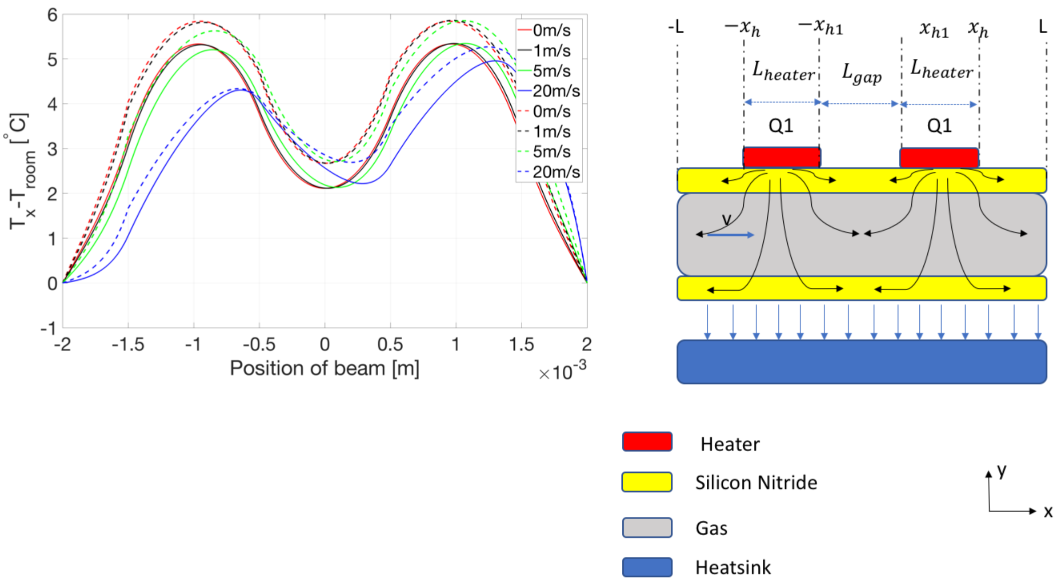

Figure 2.20: Left: the simulation result of Comsol and Matlab,the dash line indicates the simulation result and the solid ones indicates the analytical model. At $v = 0m/s$,$v = 1m/s$,$v = 5m/s$ and $v = 20m/s$, the relative average temperature difference is 5.17%,5.17%,5.45% and 6%. Right:the overview of the simulation schematic.

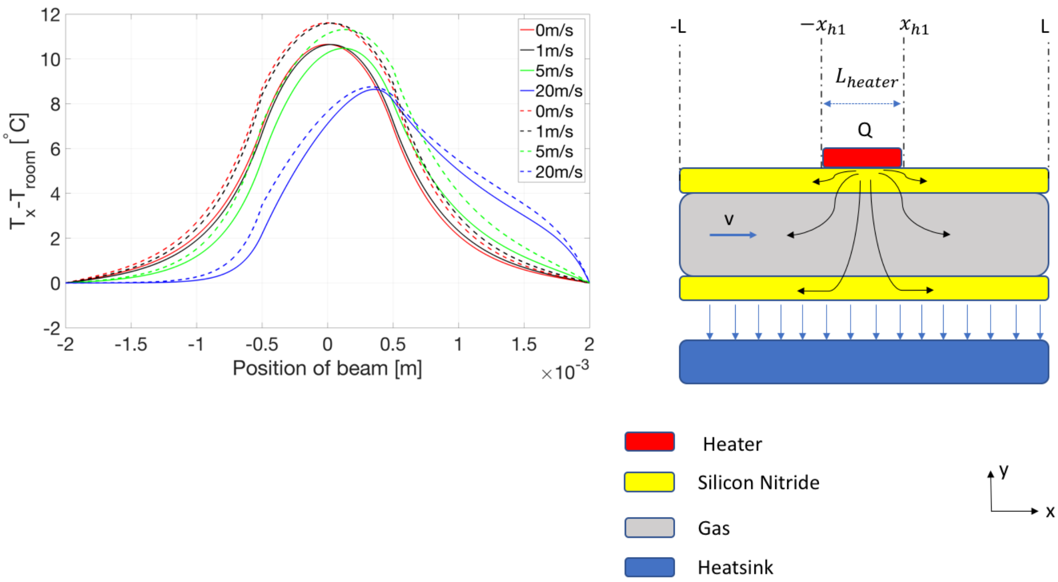

Figure 2.21: Left: the simulation result of Comsol and Matlab,the dash line indicated the simulation result whereas the solid ones denote the analytical model.At $v = 0m/s$,$v = 1m/s$,$v = 5m/s$ and $v = 20m/s$, the relative average temperature difference is 6%,6%,7.3% and 6.5%. Right:the overview of the simulation schematic.

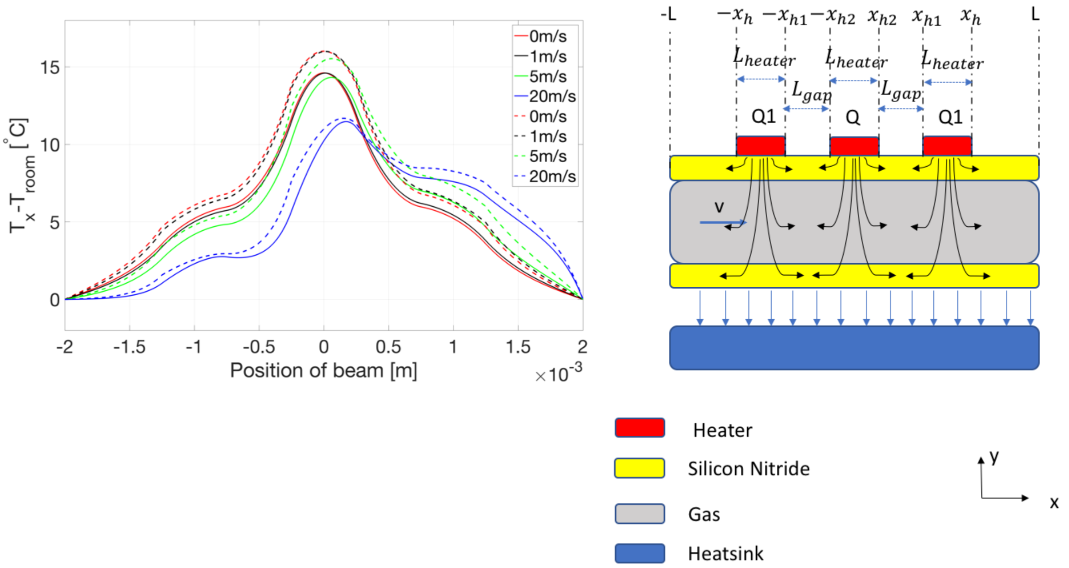

Figure 2.22: Left: the simulation result of Comsol and Matlab,the dash line indicated the simulation result whereas the solid ones denote the analytical model.At $v = 0m/s$,$v = 1m/s$,$v = 5m/s$ and $v = 20m/s$, the relative average temperature difference is 5.6%,5.6%,6.2% and 4.7%. Right:the overview of the simulation schematic.

The figure2.18, 2.20 and 2.22 shows the simulation result from Comsol and Matlab, the result of both simulations are in close agreement with each other.

2.5 Overview

In this chapter the basic theory and simulation are introduced, the result of the analytical model and Comsol model is quite fit each one, and compare to the Comsol model the simulation time of analytical model is much less. Thus if the analytical model also agrees with measurement results, this model can be used to find the optimal parameters to design a better thermal flow. Then the next chapter will show the thermal flow sensor provide by Bronkhorst, and the measurement result will be compared with the numerical simulation result to see how closely they are.

Chapter 3

Bronkhorst Sensors

This chapter describes the design, simulation, fabrication, and characterization of the thermal flow sensor developed in collaboration with the Bronkhorst. The section ends with a discussion of the results and suggestions for the new thermal flow sensor.

3.1 Design

There are three types of the sensor designed by Bronkhorst, and all of them have two heaters on the channel, which can heat the channel up and measure the temperature changes. The next section will describe the important structures of each sensor.

3.1.1 The design with different diameters of channel

Firstly, the thermal flow sensor with different channel diameters will be introduced, see figure 3.1. The important structures are denoted as:

1. The channel with 31 um radius.
2. The channel with 45 um radius.
3. The channel with 55 um radius.
4. Inlet.
5. Outlet.
6. Pressure sensor.
7. Pressure sensor.

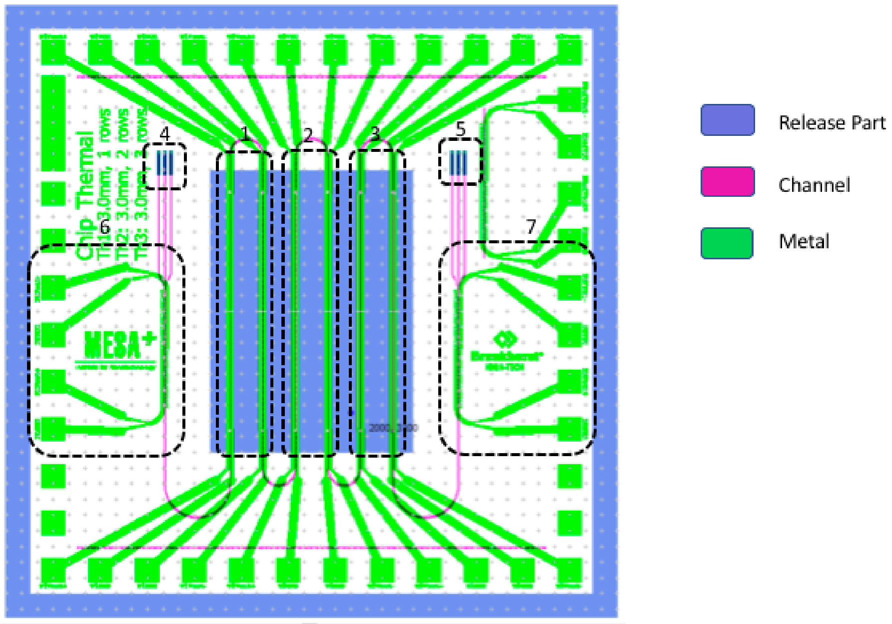

Figure 3.1: The sensor with different channel diameters, the dash block 1 is the channel with 31.5 um, the dash block 2 is the channel with 45 um and the last one is the channel with 55 um.

To fabricate the channel with different radii, different densities of patterns (purple) will be used on the device layer, see figure 3.2.The design parameters can be found in table 3.1.

Parameters	Value	Unit
Heater's dimension($H_{heater} * W_{heater} * L_{heater}$)	$0.2 \times 95 \times 1500$	um
Resistance of heater	500	Ω
Tube length	4000	um
Radius of channel 1	31.5	um
Radius of channel 2	45	um
Radius of channel 3	55	um

Table 3.1: The design parameter for thermal flow sensor with different diameters

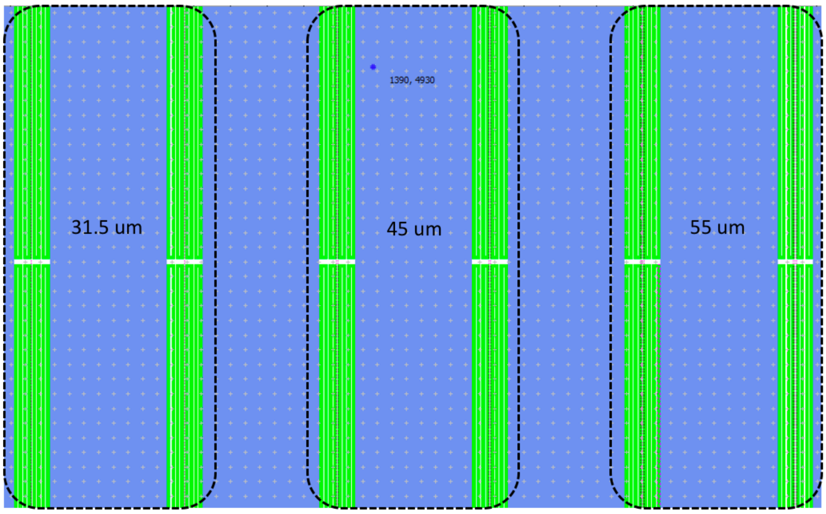

Figure 3.2: The overview of the schematics of the channels. The channel with 31.5 um radius have one line patterns on the device layer, the channel with 45 um radius have two lines patterns on the device layer and the channel with 55 um radius have three lines patterns on the device layer.

3.1.2 The Sensor with Different Heater Length

In this section, the sensor with different heater's length will be presented. Under the same supply voltage, the short heater will generate more power than the long heater. The sensor is designed as figure 3.3. The important structures are denoted as:

1. The heater with 500 um .
2. The heater with 1000 um radius.
3. The heater with 1500 um radius.
4. Inlet.
5. Outlet.
6. Pressure sensor.
7. Pressure sensor.

The specific parameters can be found in table 3.3.

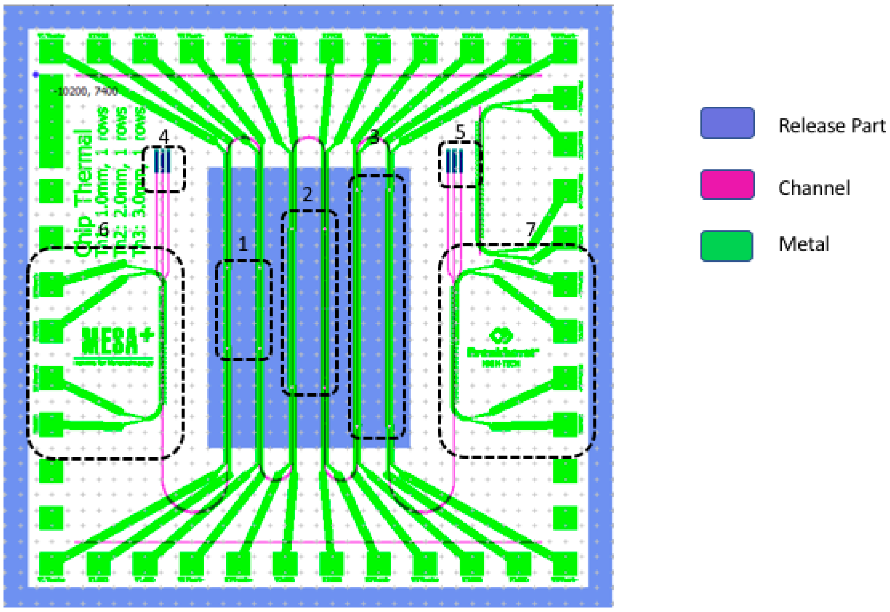

Figure 3.3: The sensor with different heater length. The dash block 1 is the channel with 500 um heater, the dash block 2 is the channel with 1000 um heater and the dash block 3 is the channel with 1500 um.

Parameters	Value	Unit
Heater1's dimension($H_{heater} * W_{heater} * L_{heater}$)	$0.2 \times 95 \times 500$	um
Resistance of 500 um heater	200	Ω
Heater2's dimension($H_{heater} * W_{heater} * L_{heater}$)	$0.2 \times 95 \times 1000$	um
Resistance of 1000 um heater	350	Ω
Heater3's dimension($H_{heater} * W_{heater} * L_{heater}$)	$0.2 \times 95 \times 1500$	um
Resistance of 1500 um heater	500	Ω
Radius of channel	31.5	um

Table 3.2: The design parameter for thermal flow sensor with different heater's length

3.1.3 The design with parallel channels

The third sensor is designed with several parallel channels, the purpose of this design is to reduce the pressure drop of fluid and increase the measurement range. For each channel, there is the $1500um$ heater replace on the channel. The sensor layout is shown in figure 3.4, and the important structures are denoted as:

1. 3 Parallel Channels .
2. 5 Parallel Channels .
3. Pressure Sensor.
4. Pressure Sensor.
5. Inlet.
6. Outlet.

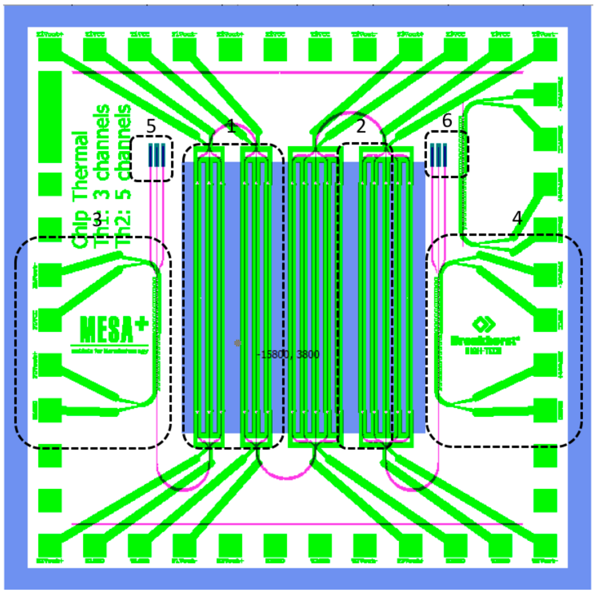

Figure 3.4: The sensor with parallel channels.

The specific parameters can be found in table 3.3.

Parameters	Value	Unit
Heater's dimension($H_{heater} * W_{heater} * L_{heater}$)	$0.2 \times 95 \times 500$	um
Resistance of 3 parallel channel	1500	Ω
Resistance of 5 parallel channel	2500	Ω
Tube length	4000	um
Radius of channel	31.5	um

Table 3.3: The design parameter for thermal flow sensor with parallel channels

3.2 Fabrication Process

Figures 3.5 , 3.6 and 3.7 show the fabrication process of the sensor. The process starts with depositing SiRN layer by using low-pressure chemical vapor deposition. Then the chromium is sputtered to protect the SiRN during the channel etch. Next, a photoresist layer is deposited and patterned; the pattern will determine the shape and size of the channel. The channel will be etched by using a semi-isotropic SF_6. Then the resist and chromium will be removed. Instead, a layer of silicon dioxide is deposited by using LPCVD, and the silicon dioxide layer will prevent etching the channel during the inlet and outlet etch.

The inlet and outlet are etched by using reactive-ion etching(DRIE), and the silicon dioxide layer will protect the channel from etching. Next, the silicon dioxide is removed using wet etch, and the SiRN layer is deposited to cover the channel and access, using LPCVD. Afterwards, a 200 nm thick metal layer is sputtered at the topside of the channel. Last, the channel is released from the bulk.

Figure 3.5: The legend of fabrication process.The picture is taken from paper [3]

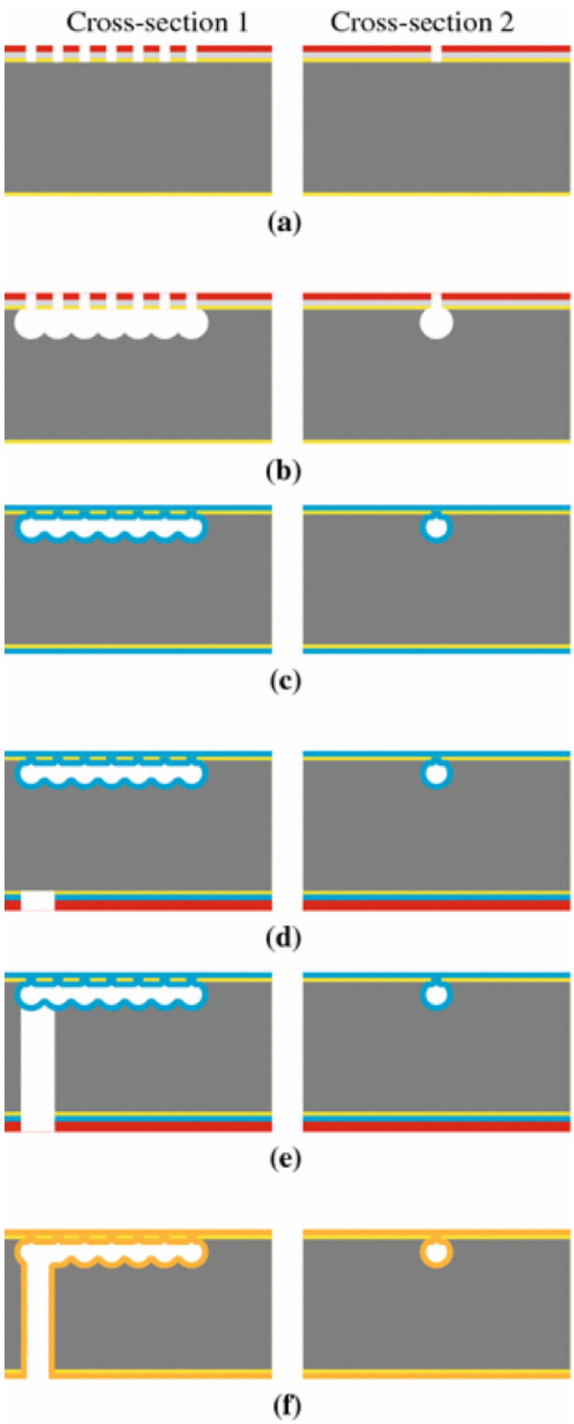

Figure 3.6: The overview of the fabrication process. The picture is taken from paper [3]

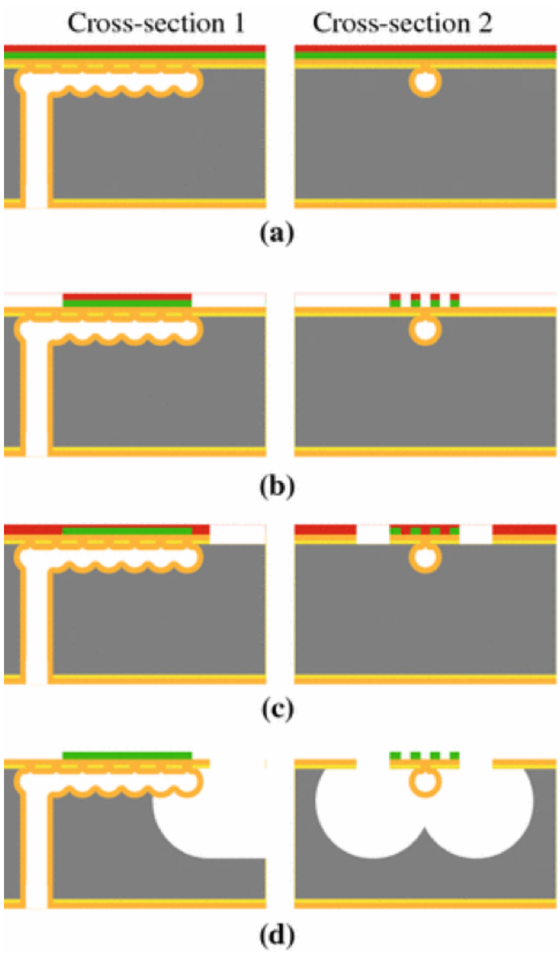

Figure 3.7: The overview of the fabrication process. The picture is taken from paper [3]

3.3 Specific readout design

In the real design, there are four heaters assembled on one ”U” shaped tube as is shown in figure 3.8, and all heaters will heat up to the same temperature when there is no flow applied. As applying the flow, the distribution of temperature will be shifted in the flow direction. This temperature shift will change the heater’s resistance which can be described as following equation [8] [9]:

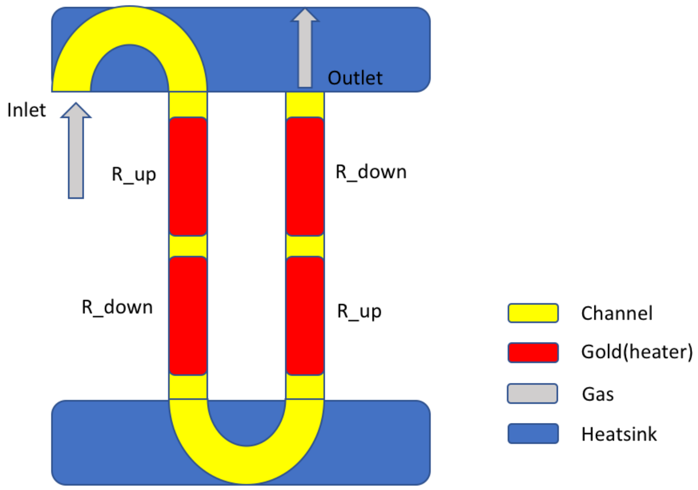

Figure 3.8: The configuration of the channel, in the figure the red part is the heater and measurement resistor, and these four heaters will be connected as Wheatone Bridge

$$R(T) = R_0[1 + \alpha\Delta T] \tag{3.1}$$

$$\Delta T = \frac{\Delta R}{\alpha R_0} \tag{3.2}$$

Where the R_0 is the heater’s resistance at $T = T_{room}$, ΔT the temperature difference between T and T_{room}, and α the temperature coefficient of resistance of the heater.

To measure the resistance changes in the equation 3.2, the Wheatstone-bridge will be used. Figure 3.9 shows the configuration of the circuit and the mathematical equations of this circuit can be described as following:

$$V_{output} = \left(\frac{R_{down}}{R_{down} + R_{up}} - \frac{R_{up}}{R_{down} + R_{up}}\right) * V_{bridge} \tag{3.3}$$

To simplify the equation 3.3, the R_{down} and R_{up} can be described as:

$$R_{up} = R_0 + \Delta T_{up} \alpha R_0 \tag{3.4}$$

$$R_{down} = R_0 + \Delta T_{down} \alpha R_0 \tag{3.5}$$

Where ΔT_{down} and ΔT_{up} is the average temperature difference on the upstream and downstream. Then the equation 3.3 can be described :

$$V_{output} = V_{bridge} * \frac{(\Delta T_{down} - \Delta T_{up})\alpha}{2 + (\Delta T_{down} + \Delta T_{up})\alpha} \tag{3.6}$$

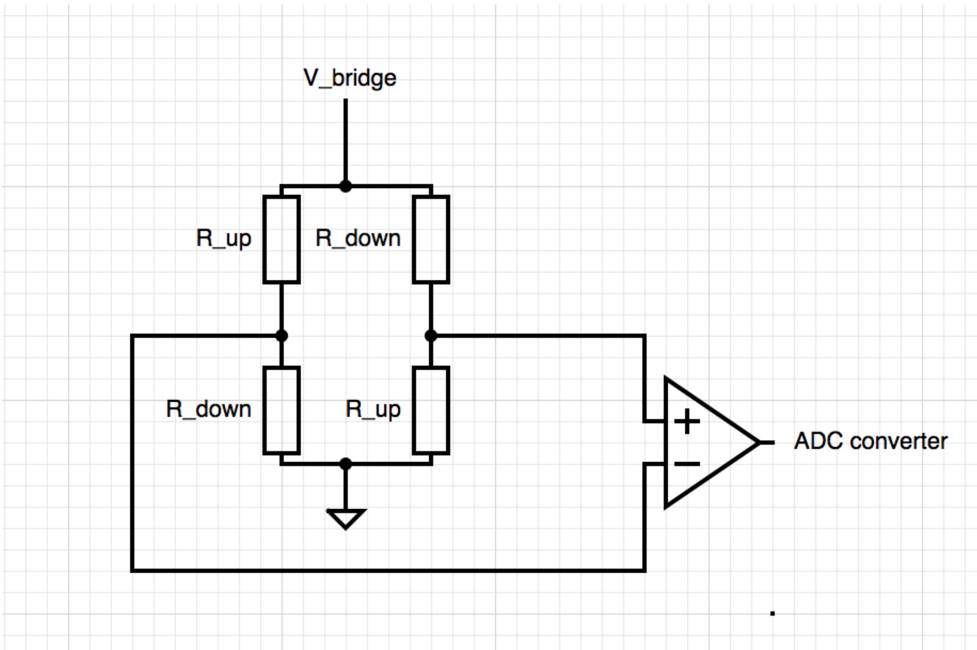

Figure 3.9: The Wheatstone bridge circuit to measure the change in resistance. The R_{up} indicates the heater placed on the up-stream and R_{down} indicates the heater placed on the down-stream. The amplifier can amplify the signal up to 150 times.

3.4 Measurement Result

In this section, the measurement result will be presented and compared to the simulation result. The silicon nitride layer and the gold layer are regarded as thin film material. Then in the later on in simulation, the thermal conductivity of silicon nitride will be 3 W/Km [10]. The TCR of gold is $0.00147/K$ which comes from measuring.

Furthermore, the sensor with parallel channels is not working during the measurement, in this section, only the results coming from the working sensor will be presented and discussed. To compare the different simulation results, all the simulations will use the same volumetric flow rate as the measurement. Again, we will subtract the simulation result from the measurement result, and divided by the maximum voltage output of Comsol to calculate the relative average voltage difference.

Some parameters will be changed to get an understanding of how they influence the sensitivity and measurement range of the sensor. Figure 3.10 shows how to define the sensitivity and measurement range of the sensor. The measurement range is the range of this linear part, and the slope of this linear line can be defined as sensitivity.

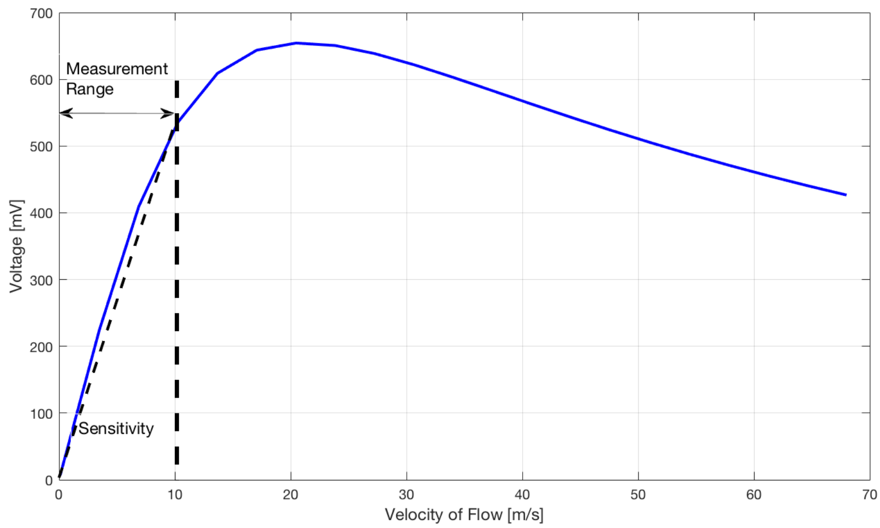

Figure 3.10: The figure of output voltage vs flow rate, the linear part which indicated by the black dash line is measurement range of sensor, and the slope of this line is the sensitivity of the sensor.

3.4.1 Simulation and Measurement Result of Sensor with Different Diameter Channel

In this section, the sensor with different diameters will be tested and simulated, to make sure the simulation is in the same conditions as the real measurement, the simulation parameters as table 3.4 will be used. Furthermore, to ensure the Matlab simulation have the proper heat-sink structure, the thermal conductance of heat-sink will directly be derived from Comsol simulation.

Parameters	Value	Unit
Thermal Conductivity of Silicon Nitride	3	W/Km
TCR of Gold	0.00147	$1/K$
Thermal Conductivity of Gold Thin Flim [11]	80	W/Km
Bridge Voltage of Wheatone Bridge	956	mV
Heater's Length	1500	um
Ambient Temperature	293.15	K
Amplification Factor	150	

Table 3.4: The Simulation Parameters

The Sensor with 31.5 um Radius Channel

The results of measurement and simulation are shown in figure 3.11.
The $G' = 14e6W/Km^3$ is derived from Comsol simulation, the Comsol simulation and Matlab simulation is close to each other, but there is an unexpected drop in flow velocity $28m/s$ and $29m/s$. To investigate the reason, we increased sweep steps and mesh density, but this unexpected drop is still in the figure, thus it might be for some specific value the Comsol can't give a proper result.

But for both simulation results, there is around 20% different from the measurement result, because the channel is placed on the position where there is a silicon wall on one side and another side is air, thus the heat-sink structure of measurement sensor is more complicated than the simulation structure. It is too difficult to build the same heat-sink structure as the actual sensor in the Comsol and Matlab.

Even for the same type of the sensor from the same wafer, the measurement are also different, figure 3.11 shows the measurement result of two sensors which are fabricated from the same wafer. As can be seen in the figure, even for the same channel design in different chip where the result is also different. Thus it is difficult to make sure all the simulation have the same heat-sink structure. But we can adjust the conductance coefficient to approximate how much they differ, figure 3.12 shows

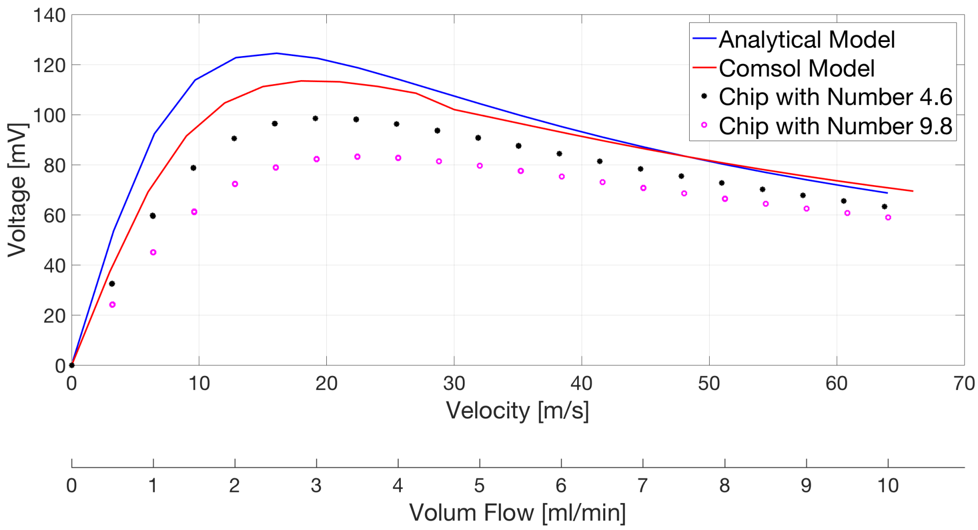

Figure 3.11: The results of different sensor for $31.5um$ radius channel. The blue line indicates the simulation result from analytical model, the red line indicates the Comsol simulation, the pink one indicates the measurement result from chip 4.6 and the black line indicates the measurement result from chip 9.8. The relative average voltage difference with respect to measurement data and analysis data of chip 4.6 is 21%, and the relative average voltage difference with respect to Comsol data and measurement data is 19%. The sensitivity of the sensor is $40.6mV/(ml/min)$ and the measurement range is $1.5ml/min$.

the measurement result and Matlab result with adjusted conductance coefficient with $\boldsymbol{G' = 19e6W/Km^3}$.

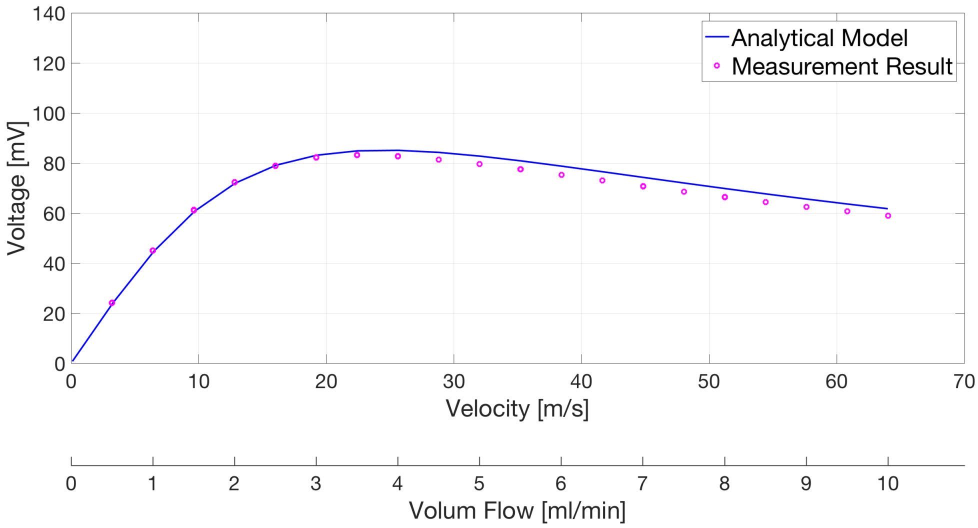

Figure 3.12: The result of analytical model and measurement, the blue line indicates the result of analytical Model and the pink point is the measurement result. In this simulation $\boldsymbol{G' = 19e6W/Km^3}$.The relative average voltage difference is $\mathbf{2.4\%}$

The Sensor with 45 um Radius Channel

The results of the channel with $45um$ radius channel is shown in figure 3.13, The $G' = 8.7e6W/Km^3$. From the figure, it can be seen that the difference between measurement value and simulation is smaller than the sensor with $45um$ radius channel. Since the $G' = G/A_{cross}$, as the radius of the channel increases, the thermal conductivity line increases, and meanwhile the cross-section area increases, but when the change rate of the cross section is bigger than the change rate of thermal conductivity, then the cross-section area will dominate the equation. This changes will result in the G' decrease. Thus there is less influence from the heat-sink structure.

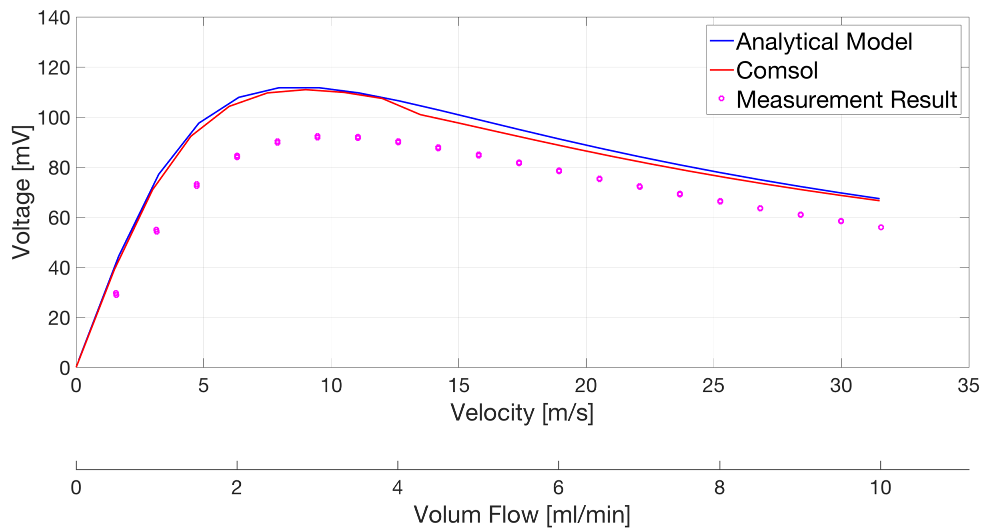

Figure 3.13: The results of simulation and measurement for $45um$ radius channel. The blue line indicates the simulation result from analytical model, the red line indicates the Comsol simulation and the black one indicate the measurement result. The relative average voltage difference with respect to measurement data and analysis data is 12%, and the relative average voltage difference with respect to Comsol data and measurement data is 11%.The sensitivity of the sensor is $48mV/(ml/min)$ and the measurement range is $1.5ml/min$.

The Sensor with 55 um Radius Channel

This section describes how the sensitivity of the sensor is influenced by changing the heater's length. As with the previous measurement with the variation of the channel's radius, the simulation parameters should be the same for Matlab and Comsol. The table 3.5 shows the simulation parameters. Furthermore, the G' will also directly derived from Comsol simulation.

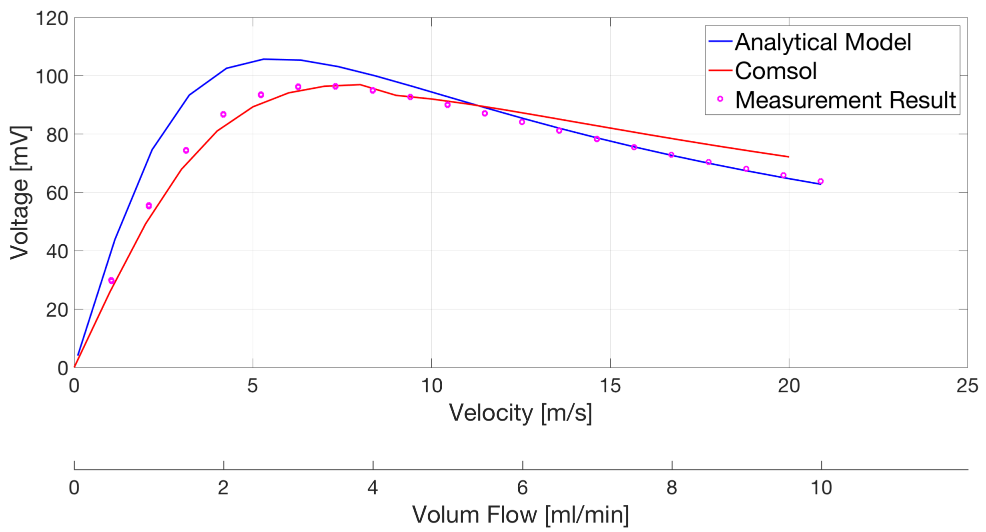

Figure 3.14: The results of simulation and measurement for $55um$ radius channel. The blue line indicates the simulation result from analytical model, the red line indicates the Comsol simulation and the black one indicate the measurement result. The relative average voltage difference with respect to measurement data and analysis data is 6.18%, and the relative average voltage difference with respect to Comsol data and measurement data is 5.14%.The sensitivity of the sensor is $50mV/(ml/min)$ and the measurement range is $1.5ml/min$.

3.4.2 Simulation and Measurement Result of Sensor with Different Heater Length

In this section, we will change the heater's length to investigate how it will influence the sensitivity of the sensor. As with the previous measurement with the variation of the channel's radius, the simulation parameters should be the same for Matlab and Comsol. But in this section, as the length of heater decreases, the resistance of heaters will decreases as well, and the heater can generate more power. The table 3.5 shows the simulation parameter. Furthermore, the heat-sink conductance will also directly derived from Comsol simulation.

Parameters	Value	Unit
Thermal Conductivity of Silicon Nitride	3	W/Km
TCR of Gold	0.00147	$1/K$
Thermal Conductivity of Gold Thin Flim [11]	80	W/Km
Radius of Channel	31.5	um
Bridge Voltage of Wheatone Bridge	956	mV
Power of $1500um$ heater	0.418	mW
Power of $1000um$ heater	0.595	mW
Power of $500um$ heater	0.8272	mW
Ambient Temperature	293.15	K
Amplification Factor	150	

Table 3.5: The Simulation Parameters For The Sensor With Different heater's length

The Sensor with 1500 um heater length

Firstly, the sensor with 1500 um heater will be measured. The figure 3.15 shows the simulation result and measurement result. Because of the difference of heat-structure between the simulation model and sensor, there still is some difference between the simulation result and measuring result. The figure 3.16 shows the simulation result of the adjusted heat-sink value, the $G' = 18e6W/Km^3$, and the relative average voltage difference is 1.5%.

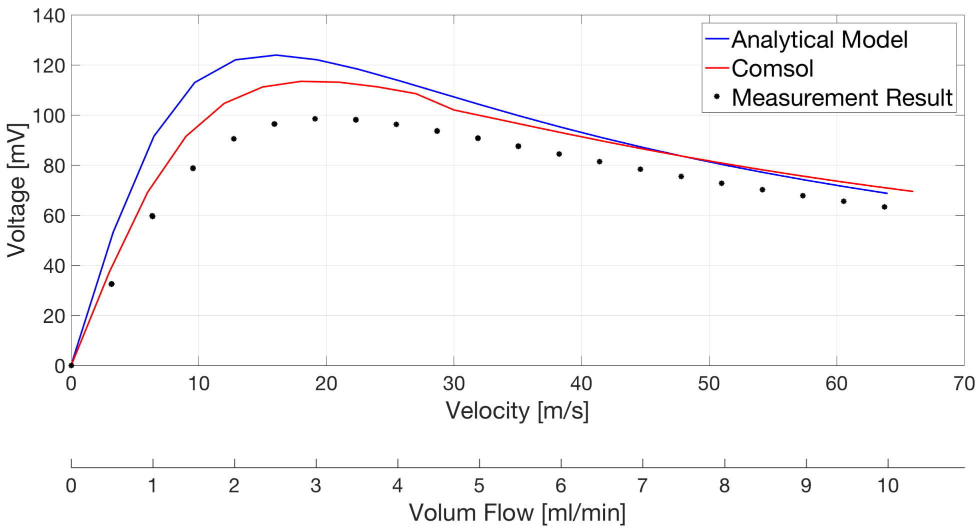

Figure 3.15: The result of simulation and measurement for the sensor with $1500um$ heater.The blue line indicates the simulation result from analytical model, the red line indicates the Comsol simulation and the black one indicate the measurement result. The relative average voltage difference with respect to measurement data and analysis data is 12.68%, and the relative average voltage difference with respect to Comsol data and measurement data is 9.2%.The sensitivity of the sensor is $52mV/(ml/min)$ and the measurement range is $1.5ml/min$.

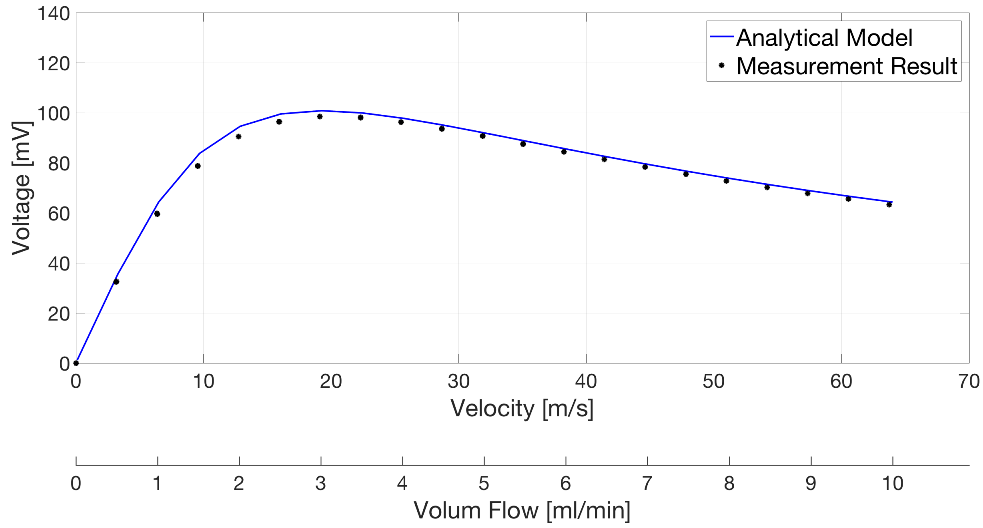

Figure 3.16: The result of Matlab Model and measurement, the blue line indicates the result of Matlab Model and the pink line is the measurement result. In this simulation the conduction of heat sink is $\mathbf{18e6W/Km^3}$, and the relative average voltage difference is 1.5%

The Sensor with 1000 um heater length

Secondly, the sensor with 1000 um heater length is simulated and measured. The figure 3.17 shows the simulation and measuring result. Compared to the sensor with 1500 um heater length, the sensitivity of the sensor is improved, because the heat flux density is increasing as the length of heater decreasing. But there still some difference between the simulation result and measurement result, because of the difference of the heat-sink structure. But compared to the sensor with 1500 um channel length, the influence of the heat-sink structure is decrease when the heater becomes shorter.

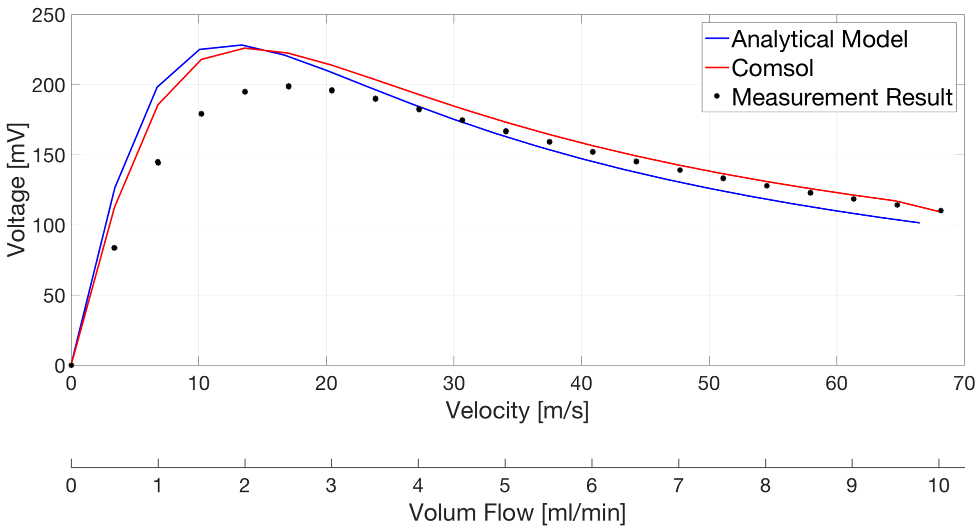

Figure 3.17: The result of simulation and measurement for the sensor with $1000um$ heater.The blue line indicates the simulation result from analytical model, the red line indicates the Comsol simulation and the black one indicate the measurement result. In this simulation the $G' = 15.4e6W/Km^3$.The relative average voltage difference with respect to measurement data and analysis data is 6.2%, and the relative average voltage difference with respect to Comsol data and measurement data is 5.2%.The sensitivity of the sensor is $118mV/(ml/min)$ and the measurement range is $1.5ml/min$.

The Sensor with 500 um heater length

The last sensor is fabricated with 500 um heater length, the simulation and measurement result can be found in figure 3.18. The $G' = 15.4e6W/Km^3$. When the heater becomes shorter, the temperature difference between the upstream heater and downstream heater is increasing in length. Meanwhile, the sensitivity is also increasing. The relative average voltage difference between the simulation result and the measurement result is 7% (Analytical model) and 5.14%(Matlab model).

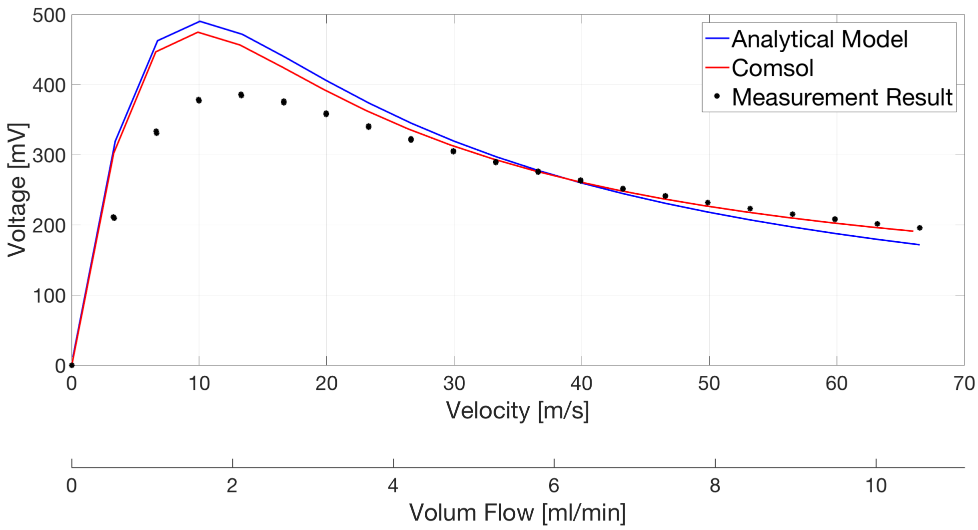

Figure 3.18: The result of simulation and measurement for the sensor with $500um$ heater.The blue line indicates the simulation result from analytical model, the red line indicates the Comsol simulation and the black one indicate the measurement result. The relative average voltage difference with respect to measurement data and analysis data is 7%, and the relative average voltage difference with respect to Comsol data and measurement data is 5.14%.The sensitivity of the sensor is $250mV/(ml/min)$ and the measurement range is $1.5ml/min$.

3.5 The Prediction of Parameter's Influence

An excellent thermal flow sensor should have high sensitivity, large measurement range, and low-pressure drop. In the last sections, we have already investigated the how the behavior of sensor changes with changing radius and heater's length. However, there are still a lot of parameters that can influence the performance of the sensor. For example, the position of the heater can be adjusted, the channel length can be adjusted, etc. In this section, we will change some parameters to see how it influence the behavior of the sensor.

3.5.1 Distance Between Heaters

Firstly, the distance between the two heaters will be adjusted to investigate how it influences the performance of the sensor. The simulation parameters will be the same as the sensor with $1500um$, $1000um$ and $500um$ the heater length which presented in the last section, and the distance between two heaters will be changed from $0um$ to $200um$. The table 3.6 shows the simulation parameters.

Parameters	Value	Unit
Thermal Conductivity of Silicon Nitride	3	W/Km
TCR of Gold	0.00147	$1/K$
Thermal Conductivity of Gold Thin Flim [11]	80	W/Km
Radius of Channel	31.5	um
Bridge Voltage of Wheatone Bridge	956	mV
Ambient Temperature	293.15	K
Amplification Factor	150	

Table 3.6: The simulation parameters for the model with changing distance between two heaters.

From the figure 3.19, as the distance between heaters increases, the sensitivity of the sensor will decreases. The reason behind it is as the distance between the heaters increase, the temperature drop between the two heaters will also increase, the temperature profile shows in appendix D.

Then to design a high sensitivity thermal flow sensor, the gap between the two heaters should be as small as possible. Otherwise, there is more heat loss due to the heat-sink. Or we can design the thermal flow sensor with only one heater placed in the middle of the channel.

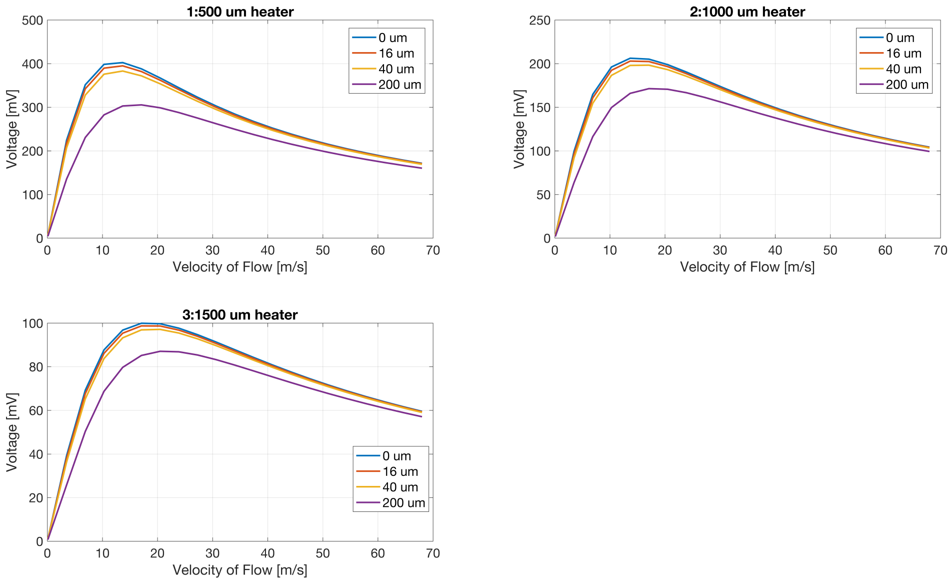

Figure 3.19: The simulation result with changing the distance between the two heaters. The first figure is the heater with 500 um length, and the distance is changed from 0 um to 200 um. The second figure is the sensor with 1000 um heater and the third one is the sensor with 1500 um heater.

3.5.2 Channel length

In the analytical model, the length of the channel is one of the variables in the heat equation. Thus it is interesting to know how the length of the channel influences the sensitivity. Firstly the simulation parameters will be defined, the heater's length will be chosen as $500um$ and without any gap between two heaters, and the length of the channel will changes from 4000 to 1000 um. And the rest of the parameters will be the same as 3.6.

Figure 3.20 shows the simulation result. For the 4000 um, 3000 um and 2000 um, the output voltage remains at same level. But from the 1800 um, the output voltage is lower. Because as the channel length decreases, the heater is closer to the boundary of the channel, then the heat-sink will force the temperature level drop to the room temperature. To have a better understanding about how the heat-sink forces the temperature to the room temperature, Appendix E shows the temperature profiles. As the output voltage decreases, the sensitivity of the sensor is also decreasing, then to design a high sensitivity sensor, the silicon heat-sink should keep some distance from heaters.

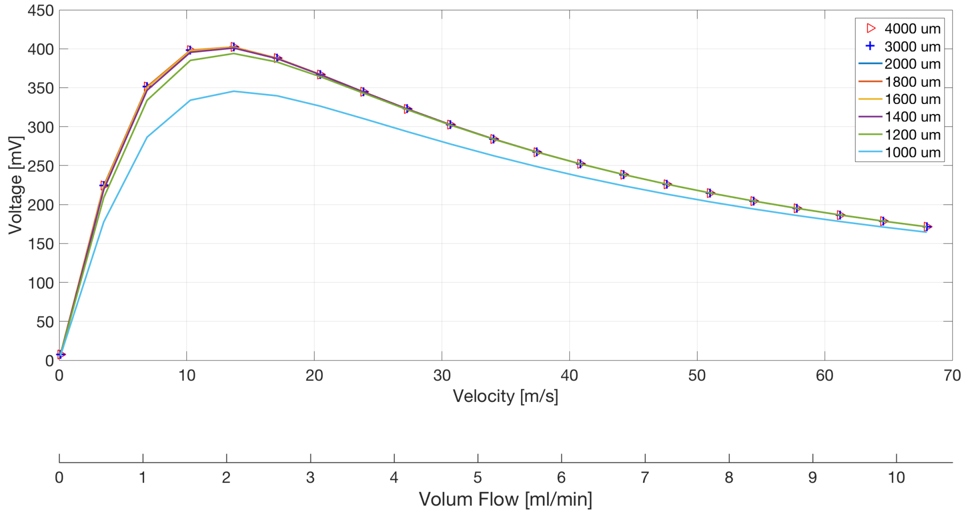

Figure 3.20: The simulation results of changing channel length. The triangle mark is the sensor with 4000 um channel length, the blue cross is the sensor with 3000 um channel length, the blue solid line is the sensor with 2000 um channel length and red line is s the sensor with 1000 um

3.5.3 How the fabrication process influence the performance

During the fabrication process, it is difficult to make sure the thickness of the material is the same as it supposes to be. Since some material such as the heater and the SiRN wall are regarded as thin film material,the changing the thickness will cause the properties of the material to change. Thus, in this section, we will investigate how the material properties influences the performance of the sensor. The simulation parameters can be found in table 3.7.

Parameters	Value	Unit
G'	20	$W/(km^3)$
Radius of Channel	31.5	um
Length of heater	500	um
Length of Channel	2000	um
Bridge Voltage of Wheatone Bridge	956	mV
Ambient Temperature	293.15	K
Amplification Factor	150	

Table 3.7: The simulation parameters for changing the material's property.

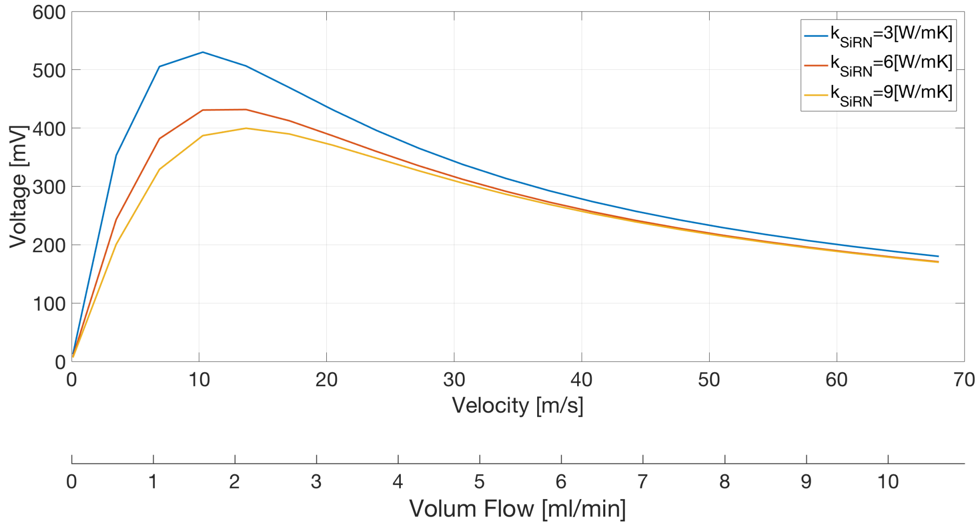

Figure 3.21: The simulation result of changing effective thermal conductivity.

Firstly, the thermal conductivity of SiRN will increase from $\mathbf{3W/mK}$ to $\mathbf{9W/mK}$. The figure 3.21 shows the simulation result, as the thermal conductivity of SiRN increases the sensitivity of the sensor decrease.

Secondly, the TCR of the gold heater is also relevant, because it will influence the resistance of the measuring resistor. Thus we will increase the TCR of gold to see how it will affect the performance of the sensor, see figure 3.22. As the TCR of gold decrease, the sensitivity of the sensor is decreasing.

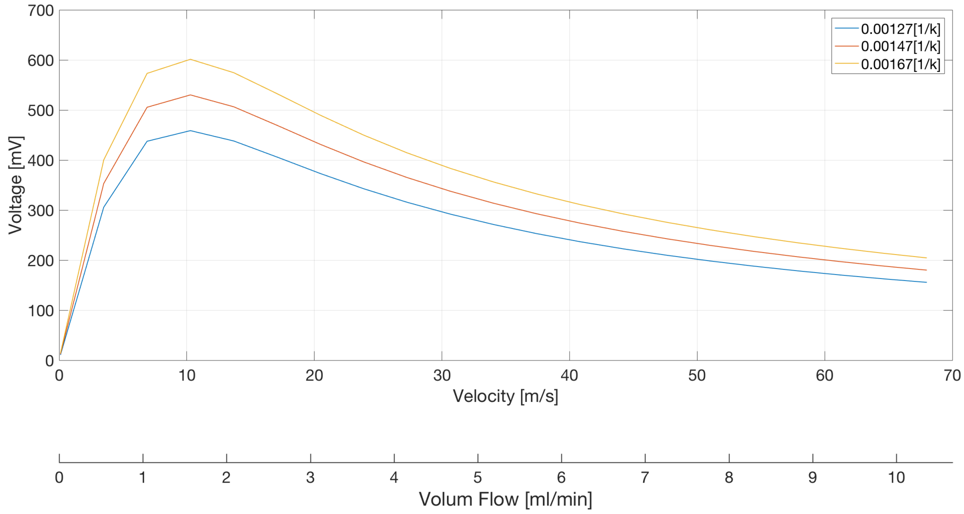

Figure 3.22: The simulation result of changing TCR of gold.

3.6 Overview

This chapter presents both simulation results and the measurement results. There still some differences between the simulation results and measurement results. The reason behind it is we can't build the same heat-sink structure as the real sensor, and calculation value of the G' will be different from the actual sensor. However, we can adjust the G' to fit the measurement result, which also means if we can get the accurate value for the conductivity of heat-sink, the simulation model can predict the output of sensor accurately.

From the simulation result of the Bronkhorst's sensor, it turns out that the sensitivity of the sensor can be improved by increasing the radius of the channel and decrease the heater's length. However, there still some parameters we can change to optimize the sensor. Later on, we also change some parameters in the simulation to investigate how it influences the sensor. First, we adjusted the distance between the two heaters, from the simulation result, the sensitivity of the sensor is improved by decreasing the distance between the two heaters. Second, when the channel's length is close to the heater's length, the sensitivity of the sensor is also decreased. What else, we also found that if the fabrication process is not accurate enough, the behavior of sensor will also change as the material's properties changes, for example, by increasing the thickness of the SiRN wall, the thermal conductivity of SiRN will be increased, it will results in the sensitivity of the sensor decrease.

Chapter 4

Conclusion and Discussion

This thesis presents two types of model to predict the behavior of a thermal flow sensor. The first model is built in Comsol, which is using numerically way to calculate the temperature profile of the sensor. The advantages of Comsol is that it can create the model in 3D, and it can use the multiple physical models. But it takes a long time to finish the simulation, especially if there is any thin film structure in the model, we must increase the mesh size to get an accurate result, and it will result in even longer time consumption. The second model is an analytical model which based on the heat equation. The advantage of the analytical model is that it takes much less time to generate the result, and the result is close to the Comsol simulation.

Later on, the sensors from the Bronkhorst are measured to verify the simulation results. The simulation result is close to the measurement result, but there is some difference between the simulation result and measurement result. The main reason behind it is that the heat structure in the actual sensor is too complex to construct it in the simulation. Meanwhile, we also investigate how the design parameters will influence the behavior of the thermal flow sensor. From the simulation and measurement result in chapter 3.4.1, the sensitivity of the sensor increases as the radius increases. For example, the sensitivity of the sensor with $31.5um$ radius channel is $40.6mV/(ml/min)$, when we increase the radius of channel to $45um$, the sensitivity now is $48mV/(ml/min)$. In the chapter 3.4.2, the sensitivity of the sensor can be improved by decreasing the heater's length. For example, the sensitivity of the sensor with $1000um$ heater is $118mV/(ml/min)$, the sensitivity of the sensor with $500um$ heater is $250mV/(ml/min)$. Except for these two parameters, there still have some parameters can influence the behavior of the sensor. Thus, in chapter 3.5, we run the analytical model by adjusting some design parameters, such as the distance between two heaters, channel length, and material properties. It turns out that increasing the distance of two heaters, decreases the channel length and increases the thickness of SiRN will result in decreasing the sensitivity. By collecting all these information, the new thermal sensor with one heater is designed. But due to the time limitation, we design a mask but doesn't fabrication out, see the appendix F.

Chapter 5

Outlook on future work

In this thesis, the analytical model is built to predict the behavior of the thermal flow sensor, but there are some items remain to be done:

1. The equation to approximate the G' in this thesis is not accurate enough, therefore it is important to find a proper way to calculate the G'.
2. Except the design parameters mentioned in this thesis, there still have some design parameters can be investigated, for example, it might help to place the sensor in the vacuum, the sensitivity might be improved by applying more heaters, the measurement range might be an increase by using multiple channels, etc.
3. Base on the analytical model in this thesis, it might be interesting to develop a software can generate omptimal design parameter when we enter the sensitivity and measurement range.

Bibliography

[1] “Comsol, inc.” https://www.comsol.com/.

[2] “Ansys, inc.” https://www.ansys.com/.

[3] J. Groenesteijn, M. J. de Boer, J. C. Lötters, and R. J. Wiegerink, “A versatile technology platform for microfluidic handling systems, part i: fabrication and functionalization,” *Microfluidics and Nanofluidics*, vol. 21, no. 7, p. 127, Jul 2017. [Online]. Available: https://doi.org/10.1007/s10404-017-1961-0

[4] “Bronkhorst nederland b.v.” https://www.bronkhorst.nl/.

[5] H.H.Bruun., *Hot-Wire Anemometry*. Oxford University Press, 1994.

[6] “Wolfram research corp.” http://www.wolfram.com/.

[7] T. L. B. A. S. L. Frank P. Incropera, David P. Dewitt, *Fundamentals of Heat and Mass Transfer*. JOHN WILEY SONS, 2006.

[8] K. Ohe and Y. Naito, “A new resistor having an anomalously large positive temperature coefficient,” *Japanese Journal of Applied Physics*, vol. 10, no. 1, p. 99, 1971.

[9] A. Alenitesyn and E. Butikov, “. concise handbook of mathematics and physics.” *CRC Press (Boca Raton, Fla. and Moscow)*, 1997.

[10] C. H. Mastrangelo, Y.-C. Tai, and R. S. Muller, “Thermophysical properties of low-residual stress, silicon-rich, lpcvd silicon nitride films,” *Sensors and Actuators A: Physical*, vol. 23, no. 1, pp. 856 – 860, 1990, proceedings of the 5th International Conference on Solid-State Sensors and Actuators and Eurosensors III. [Online]. Available: http://www.sciencedirect.com/science/article/pii/092442479087046L

[11] G. Langer, J. Hartmann, and M. Reichling, “Thermal conductivity of thin metallic films measured by photothermal profile analysis,” *Review of Scientific Instruments*, vol. 68, no. 3, pp. 1510–1513, 1997. [Online]. Available: https://doi.org/10.1063/1.1147638

Appendix A

The method to solve the constants

In this section, we will present the way to solve the equation 2.23 to 2.28 in section 2.1:

$$A_1 e^{-rL} + B_1 = A_2 e^{rL} + B_2 = T_{heatsink} \tag{A.1}$$

$$A_1 e^{-rx_h} + B_1 = C_1 e^{-rx_h} + C_2 - \frac{Qx_h}{rk} \tag{A.2}$$

$$A_2 e^{rx_h} + B_2 = C_1 e^{rx_h} + C_2 + \frac{Qx_h}{rk} \tag{A.3}$$

$$A_1 r e^{-rx_h} = C_1 r e^{-rx_h} + \frac{Q}{rk} \tag{A.4}$$

$$A_2 r e^{rx_h} = C_1 r e^{rx_h} + \frac{Q}{rk} \tag{A.5}$$

To solve the six constant,firstly we rewrite the equation A.1 as following:

$$A_1 e^{-rL} - A_2 e^{rL} = B_2 - B_1 \tag{A.6}$$

Then using equation A.3 minus A.2:

$$A_2 e^{rx_h} - A_1 e^{-rx_h} + A_1 e^{-rL} - A_2 e^{rL} = C_1 e^{rx_h} - C_1 e^{-rx_h} + 2\frac{Qx_h}{rk} \tag{A.7}$$

Next using equation A.5 minus A.4 to find the relation between C_1 , A_1 and A_2

$$A_2 r e^{rx_h} - A_1 r e^{-rx_h} = C_1 e^{rx_h} - C_1 e^{-rx_h} \tag{A.8}$$

Replacing the equation A.8 into A.7, the relation between A_1 and A_2 can be found as:

$$A_1 = 2\frac{Qx_h}{rke^{-rL}} + A_2 e^{2rL} \tag{A.9}$$

To solve the A_1 and A_2 we need using euqaiton A.4 and A.5 again, but before subtracting them, the equation A.4 need to divide e^{-rx_h} and the equation A.5 need to divide e^{rx_h}:

$$A_1 - A_2 = \frac{Q}{r^2ke^{-rx_h}} - \frac{Q}{r^2ke^{rx_h}} \tag{A.10}$$

Replacing equation A.9 into A.10 the A_2 can be solved as:

$$A_2 = \frac{Q(e^{-r(L-x_h)} - e^{-r(L+x_h)} - 2x_hr)}{r^2k(e^{rL} - e^{-rL})} \tag{A.11}$$

Now we have already known A_2, then the A_1 can be solved by replacing A_2 into equation A.10, C_1 can be solved by replacing A_1 and A_2 into equation A.8, and B_1 and B_2 can be solved by using equation A.1.

Appendix B

The constant for equation 2.37

This section provide the constants for the heat equation 2.37, which is located in Chapter 2.3.

It is difficult to solve the 14 variables with 14 equations, then the software called Mathematica is used to solve the equation, the PDF file attached as following shows those 14 equations and the solution of them.

$$\text{Solve}\Big[A_1 \times e^{-r*L} + B_1 == 0 \,\&\&\, A_4 \times e^{r*L} + B_4 == 0 \,\&\&$$

解方程

$$A_1 \times e^{-r*X_h} + B_1 - C_1 \times e^{-r*X_h} - C_2 + \left(Q \times X_h\right) / \left(r \times k\right) == 0 \,\&\&$$
$$A_1 \times r \times e^{-r*X_h} - C_1 \times r \times e^{-r*X_h} - \left(Q\right) / \left(r \times k\right) == 0 \,\&\&$$
$$A_2 \times e^{-r*X_{h1}} + B_2 - C_1 \times e^{-r*X_{h1}} - C_2 + \left(Q \times X_{h1}\right) / \left(r \times k\right) == 0 \,\&\&$$
$$A_2 \times r \times e^{-r*X_{h1}} - C_1 \times r \times e^{-r*X_{h1}} - \left(Q\right) / \left(r \times k\right) == 0 \,\&\&$$
$$A_2 \times e^{-r*X_{h2}} + B_2 - C_3 \times e^{-r*X_{h2}} - C_4 + \left(Q \times X_{h2}\right) / \left(r \times k\right) == 0 \,\&\&$$
$$A_2 \times r \times e^{-r*X_{h2}} - C_3 \times r \times e^{-r*X_{h2}} - \left(Q\right) / \left(r \times k\right) == 0 \,\&\&$$
$$A_3 \times e^{r*X_{h2}} + B_3 - C_3 \times e^{r*X_{h2}} - C_4 - \left(Q \times X_{h2}\right) / \left(r \times k\right) == 0 \,\&\&$$
$$A_3 \times r \times e^{r*X_{h2}} - C_3 \times r \times e^{r*X_{h2}} - \left(Q\right) / \left(r \times k\right) == 0 \,\&\&$$
$$A_3 \times e^{r*X_{h1}} + B_3 - C_5 \times e^{r*X_{h1}} - C_6 - \left(Q \times X_{h1}\right) / \left(r \times k\right) == 0 \,\&\&$$
$$A_3 \times r \times e^{r*X_{h1}} - C_5 \times r \times e^{r*X_{h1}} - \left(Q\right) / \left(r \times k\right) == 0 \,\&\&$$
$$A_4 \times e^{r*X_h} + B_4 - C_5 \times e^{r*X_h} - C_6 - \left(Q \times X_h\right) / \left(r \times k\right) == 0 \,\&\&$$
$$A_4 \times r \times e^{r*X_h} - C_5 \times r \times e^{r*X_h} - \left(Q\right) / \left(r \times k\right) == 0,$$
$$\{A_1, B_1, A_2, B_2, A_3, B_3, A_4, B_4, C_1, C_2, C_3, C_4, C_5, C_6\}\Big]$$

$$\Big\{\Big\{A_1 \to \frac{1}{\left(-1 + e^{2 L r}\right) k\, r^2} e^{L r - r X_h - r X_{h1} - r X_{h2}} Q$$
$$\Big(-e^{L r + r X_h + r X_{h1}} + e^{L r + r X_h + r X_{h2}} - e^{L r + r X_{h1} + r X_{h2}} + e^{L r + 2 r X_h + r X_{h1} + r X_{h2}} - e^{L r + r X_h + 2 r X_{h1} + r X_{h2}} +$$
$$e^{L r + r X_h + r X_{h1} + 2 r X_{h2}} - 2\, e^{r X_h + r X_{h1} + r X_{h2}} r X_h + 2\, e^{r X_h + r X_{h1} + r X_{h2}} r X_{h1} - 2\, e^{r X_h + r X_{h1} + r X_{h2}} r X_{h2}\Big),$$

$$B_1 \to -\frac{1}{\left(-1 + e^{2 L r}\right) k\, r^2} e^{-r X_h - r X_{h1} - r X_{h2}} Q \Big(-e^{L r + r X_h + r X_{h1}} + e^{L r + r X_h + r X_{h2}} - e^{L r + r X_{h1} + r X_{h2}} +$$
$$e^{L r + 2 r X_h + r X_{h1} + r X_{h2}} - e^{L r + r X_h + 2 r X_{h1} + r X_{h2}} + e^{L r + r X_h + r X_{h1} + 2 r X_{h2}} -$$
$$2\, e^{r X_h + r X_{h1} + r X_{h2}} r X_h + 2\, e^{r X_h + r X_{h1} + r X_{h2}} r X_{h1} - 2\, e^{r X_h + r X_{h1} + r X_{h2}} r X_{h2}\Big),$$

$$A_2 \to \frac{1}{\left(-1 + e^{2 L r}\right) k\, r^2} e^{-r X_h - r X_{h1} - r X_{h2}} Q \Big(-e^{2 L r + r X_h + r X_{h1}} + e^{2 L r + r X_h + r X_{h2}} - e^{2 L r + r X_{h1} + r X_{h2}} +$$
$$e^{2 r X_h + r X_{h1} + r X_{h2}} - e^{r X_h + 2 r X_{h1} + r X_{h2}} + e^{2 L r + r X_h + r X_{h1} + 2 r X_{h2}} -$$
$$2\, e^{L r + r X_h + r X_{h1} + r X_{h2}} r X_h + 2\, e^{L r + r X_h + r X_{h1} + r X_{h2}} r X_{h1} - 2\, e^{L r + r X_h + r X_{h1} + r X_{h2}} r X_{h2}\Big),$$

$$B_2 \to \frac{1}{\left(-1 + e^{2 L r}\right) k\, r^2} e^{-r X_h - r X_{h1} - r X_{h2}} Q \Big(e^{L r + r X_h + r X_{h1}} - e^{L r + r X_h + r X_{h2}} + e^{L r + r X_{h1} + r X_{h2}} -$$
$$e^{L r + 2 r X_h + r X_{h1} + r X_{h2}} + e^{L r + r X_h + 2 r X_{h1} + r X_{h2}} - e^{L r + r X_h + r X_{h1} + 2 r X_{h2}} + e^{r X_h + r X_{h1} + r X_{h2}} r X_h +$$
$$e^{2 L r + r X_h + r X_{h1} + r X_{h2}} r X_h - e^{r X_h + r X_{h1} + r X_{h2}} r X_{h1} - e^{2 L r + r X_h + r X_{h1} + r X_{h2}} r X_{h1} + 2\, e^{r X_h + r X_{h1} + r X_{h2}} r X_{h2}\Big),$$

$$A_3 \to \frac{1}{\left(-1 + e^{2 L r}\right) k\, r^2} e^{-r X_h - r X_{h1} - r X_{h2}} Q \Big(-e^{r X_h + r X_{h1}} + e^{2 L r + r X_h + r X_{h2}} - e^{2 L r + r X_{h1} + r X_{h2}} +$$
$$e^{2 r X_h + r X_{h1} + r X_{h2}} - e^{r X_h + 2 r X_{h1} + r X_{h2}} + e^{r X_h + r X_{h1} + 2 r X_{h2}} - 2\, e^{L r + r X_h + r X_{h1} + r X_{h2}} r X_h +$$
$$2\, e^{L r + r X_h + r X_{h1} + r X_{h2}} r X_{h1} - 2\, e^{L r + r X_h + r X_{h1} + r X_{h2}} r X_{h2}\Big),$$

$$B_3 \to \frac{1}{\left(-1 + e^{2 L r}\right) k\, r^2} e^{-r X_h - r X_{h1} - r X_{h2}} Q \Big(e^{L r + r X_h + r X_{h1}} - e^{L r + r X_h + r X_{h2}} + e^{L r + r X_{h1} + r X_{h2}} - e^{L r + 2 r X_h + r X_{h1} + r X_{h2}} +$$
$$e^{L r + r X_h + 2 r X_{h1} + r X_{h2}} - e^{L r + r X_h + r X_{h1} + 2 r X_{h2}} + e^{r X_h + r X_{h1} + r X_{h2}} r X_h + e^{2 L r + r X_h + r X_{h1} + r X_{h2}} r X_h -$$
$$e^{r X_h + r X_{h1} + r X_{h2}} r X_{h1} - e^{2 L r + r X_h + r X_{h1} + r X_{h2}} r X_{h1} + 2\, e^{2 L r + r X_h + r X_{h1} + r X_{h2}} r X_{h2}\Big),$$

$$A_4 \to \frac{1}{\left(-1+e^{2 L r}\right) k r^2} e^{-r X_h - r X_{h1} - r X_{h2}} Q \left(-e^{r X_h + r X_{h1}} + e^{r X_h + r X_{h2}} - e^{r X_{h1} + r X_{h2}} + e^{2 r X_h + r X_{h1} + r X_{h2}} - e^{r X_h + 2 r X_{h1} + r X_{h2}} + e^{r X_h + r X_{h1} + 2 r X_{h2}} - 2 e^{L r + r X_h + r X_{h1} + r X_{h2}} r X_h + 2 e^{L r + r X_h + r X_{h1} + r X_{h2}} r X_{h1} - 2 e^{L r + r X_h + r X_{h1} + r X_{h2}} r X_{h2}\right),$$

$$B_4 \to -\frac{1}{\left(-1+e^{2 L r}\right) k r^2} e^{L r - r X_h - r X_{h1} - r X_{h2}} Q \left(-e^{r X_h + r X_{h1}} + e^{r X_h + r X_{h2}} - e^{r X_{h1} + r X_{h2}} + e^{2 r X_h + r X_{h1} + r X_{h2}} - e^{r X_h + 2 r X_{h1} + r X_{h2}} + e^{r X_h + r X_{h1} + 2 r X_{h2}} - 2 e^{L r + r X_h + r X_{h1} + r X_{h2}} r X_h + 2 e^{L r + r X_h + r X_{h1} + r X_{h2}} r X_{h1} - 2 e^{L r + r X_h + r X_{h1} + r X_{h2}} r X_{h2}\right),$$

$$C_1 \to -\frac{1}{\left(-1+e^{2 L r}\right) k r^2} e^{-r X_h - r X_{h1} - r X_{h2}} Q \left(e^{2 L r + r X_h + r X_{h1}} - e^{2 L r + r X_h + r X_{h2}} + e^{2 L r + r X_{h1} + r X_{h2}} - e^{2 r X_h + r X_{h1} + r X_{h2}} + e^{2 L r + r X_h + 2 r X_{h1} + r X_{h2}} - e^{2 L r + r X_h + r X_{h1} + 2 r X_{h2}} + 2 e^{L r + r X_h + r X_{h1} + r X_{h2}} r X_h - 2 e^{L r + r X_h + r X_{h1} + r X_{h2}} r X_{h1} + 2 e^{L r + r X_h + r X_{h1} + r X_{h2}} r X_{h2}\right),$$

$$C_2 \to \frac{1}{\left(-1+e^{2 L r}\right) k r^2} e^{-r X_h - r X_{h1} - r X_{h2}} Q \left(e^{L r + r X_h + r X_{h1}} - e^{L r + r X_h + r X_{h2}} + e^{L r + r X_{h1} + r X_{h2}} - e^{r X_h + r X_{h1} + r X_{h2}} + e^{2 L r + r X_h + r X_{h1} + r X_{h2}} - e^{L r + 2 r X_h + r X_{h1} + r X_{h2}} + e^{L r + r X_h + 2 r X_{h1} + r X_{h2}} - e^{L r + r X_h + r X_{h1} + 2 r X_{h2}} + e^{r X_h + r X_{h1} + r X_{h2}} r X_h + e^{2 L r + r X_h + r X_{h1} + r X_{h2}} r X_h - 2 e^{r X_h + r X_{h1} + r X_{h2}} r X_{h1} + 2 e^{r X_h + r X_{h1} + r X_{h2}} r X_{h2}\right),$$

$$C_3 \to \frac{1}{\left(-1+e^{2 L r}\right) k r^2} e^{-r X_h - r X_{h1} - r X_{h2}} Q \left(-e^{2 L r + r X_h + r X_{h1}} + e^{2 L r + r X_h + r X_{h2}} - e^{2 L r + r X_{h1} + r X_{h2}} + e^{2 r X_h + r X_{h1} + r X_{h2}} - e^{r X_h + 2 r X_{h1} + r X_{h2}} + e^{r X_h + r X_{h1} + 2 r X_{h2}} - 2 e^{L r + r X_h + r X_{h1} + r X_{h2}} r X_h + 2 e^{L r + r X_h + r X_{h1} + r X_{h2}} r X_{h1} - 2 e^{L r + r X_h + r X_{h1} + r X_{h2}} r X_{h2}\right),$$

$$C_4 \to \frac{1}{\left(-1+e^{2 L r}\right) k r^2} e^{-r X_h - r X_{h1} - r X_{h2}} Q \left(e^{L r + r X_h + r X_{h1}} - e^{L r + r X_h + r X_{h2}} + e^{L r + r X_{h1} + r X_{h2}} - e^{r X_h + r X_{h1} + r X_{h2}} + e^{2 L r + r X_h + r X_{h1} + r X_{h2}} - e^{L r + 2 r X_h + r X_{h1} + r X_{h2}} + e^{L r + r X_h + 2 r X_{h1} + r X_{h2}} - e^{L r + r X_h + r X_{h1} + 2 r X_{h2}} + e^{r X_h + r X_{h1} + r X_{h2}} r X_h + e^{2 L r + r X_h + r X_{h1} + r X_{h2}} r X_h - e^{r X_h + r X_{h1} + r X_{h2}} r X_{h1} - e^{2 L r + r X_h + r X_{h1} + r X_{h2}} r X_{h1} + e^{r X_h + r X_{h1} + r X_{h2}} r X_{h2} + e^{2 L r + r X_h + r X_{h1} + r X_{h2}} r X_{h2}\right),$$

$$C_5 \to -\frac{1}{\left(-1+e^{2 L r}\right) k r^2} e^{-r X_h - r X_{h1} - r X_{h2}} Q \left(e^{r X_h + r X_{h1}} - e^{r X_h + r X_{h2}} + e^{2 L r + r X_{h1} + r X_{h2}} - e^{2 r X_h + r X_{h1} + r X_{h2}} + e^{r X_h + 2 r X_{h1} + r X_{h2}} - e^{r X_h + r X_{h1} + 2 r X_{h2}} + 2 e^{L r + r X_h + r X_{h1} + r X_{h2}} r X_h - 2 e^{L r + r X_h + r X_{h1} + r X_{h2}} r X_{h1} + 2 e^{L r + r X_h + r X_{h1} + r X_{h2}} r X_{h2}\right),$$

$$C_6 \to \frac{1}{\left(-1+e^{2 L r}\right) k r^2} e^{-r X_h - r X_{h1} - r X_{h2}} Q \left(e^{L r + r X_h + r X_{h1}} - e^{L r + r X_h + r X_{h2}} + e^{L r + r X_{h1} + r X_{h2}} - e^{r X_h + r X_{h1} + r X_{h2}} + e^{2 L r + r X_h + r X_{h1} + r X_{h2}} - e^{L r + 2 r X_h + r X_{h1} + r X_{h2}} + e^{L r + r X_h + 2 r X_{h1} + r X_{h2}} - e^{L r + r X_h + r X_{h1} + 2 r X_{h2}} + e^{r X_h + r X_{h1} + r X_{h2}} r X_h + e^{2 L r + r X_h + r X_{h1} + r X_{h2}} r X_h - 2 e^{2 L r + r X_h + r X_{h1} + r X_{h2}} r X_{h1} + 2 e^{2 L r + r X_h + r X_{h1} + r X_{h2}} r X_{h2}\right)\}\}$$

Appendix C

The constant for equation 2.46

The solution for the equation 2.46,as describe in the chapter 2.4. The constant is solved by using Mathmematica ,reads:

$$\text{Solve}\Big[A_1 \times e^{-r1*L} + B_1 \times e^{-r2*L} == 0 \,\&\&\, A_4 \times e^{r1*L} + B_4 \times e^{r2*L} == 0 \,\&\&$$

解方程

$$A_1 \times e^{-r1*X_h} + B_1 \times e^{-r2*X_h} - C_1 \times e^{-r1*X_h} - C_2 \times e^{-r2*X_h} - (Q1) / (G) == 0 \,\&\&$$
$$A_1 \times r1 \times e^{-r1*X_h} + B_1 \times r2 \times e^{-r2*X_h} - C_1 \times r1 \times e^{-r1*X_h} - C_2 \times r2 \times e^{-r2*X_h} == 0 \,\&\&$$
$$A_2 \times e^{-r1*X_{h1}} + B_2 \times e^{-r2*X_{h1}} - C_1 \times e^{-r1*X_{h1}} - C_2 \times e^{-r2*X_{h1}} - (Q1) / (G) == 0 \,\&\&$$
$$A_2 \times r1 \times e^{-r1*X_{h1}} + B_2 \times r2 \times e^{-r2*X_{h1}} - C_1 \times r1 \times e^{-r1*X_{h1}} - C_2 \times r2 \times e^{-r2*X_{h1}} == 0 \,\&\&$$
$$A_2 \times e^{-r1*X_{h2}} + B_2 \times e^{-r2*X_{h2}} - C_3 \times e^{-r1*X_{h2}} - C_4 \times e^{-r2*X_{h2}} - (Q) / (G) == 0 \,\&\&$$
$$A_2 \times r1 \times e^{-r1*X_{h2}} + B_2 \times r2 \times e^{-r2*X_{h2}} - C_3 \times r1 \times e^{-r1*X_{h2}} - C_4 \times r2 \times e^{-r2*X_{h2}} == 0 \,\&\&$$
$$A_3 \times e^{r1*X_{h2}} + B_3 \times e^{r2*X_{h2}} - C_3 \times e^{r1*X_{h2}} - C_4 \times e^{r2*X_{h2}} - (Q) / (G) == 0 \,\&\&$$
$$A_3 \times r1 \times e^{r1*X_{h2}} + B_3 \times r2 \times e^{r2*X_{h2}} - C_3 \times r1 \times e^{r1*X_{h2}} - C_4 \times r2 \times e^{r2*X_{h2}} == 0 \,\&\&$$
$$A_3 \times e^{r1*X_{h1}} + B_3 \times e^{r2*X_{h1}} - C_5 \times e^{r1*X_{h1}} - C_6 \times e^{r2*X_{h1}} - (Q1) / (G) == 0 \,\&\&$$
$$A_3 \times r1 \times e^{r1*X_{h1}} + B_3 \times r2 \times e^{r2*X_{h1}} - C_5 \times r1 \times e^{r1*X_{h1}} - C_6 \times r2 \times e^{r2*X_{h1}} == 0 \,\&\&$$
$$A_4 \times e^{r1*X_h} + B_4 \times e^{r2*X_h} - C_5 \times e^{r1*X_h} - C_6 \times e^{r2*X_h} - (Q1) / (G) == 0 \,\&\&$$
$$A_4 \times r1 \times e^{r1*X_h} + B_4 \times r2 \times e^{r2*X_h} - C_5 \times r1 \times e^{r1*X_h} - C_6 \times r2 \times e^{r2*X_h} == 0,$$
$$\{A_1, B_1, A_2, B_2, A_3, B_3, A_4, B_4, C_1, C_2, C_3, C_4, C_5, C_6\}\Big]$$

$$\Big\{\Big\{A_1 \to -\frac{1}{\left(-e^{2 L r1} + e^{2 L r2}\right) G \left(r1 - r2\right)}$$
$$e^{-r1 X_h - r2 X_h - r1 X_{h1} - r2 X_{h1} - r1 X_{h2} - r2 X_{h2}} \Big(-e^{L r1 + L r2 + r1 X_h + r2 X_h + r1 X_{h1} + r2 X_{h1} + r1 X_{h2}} Q\, r1 +$$
$$e^{L r1 + L r2 + r1 X_h + r2 X_h + r1 X_{h1} + r2 X_{h1} + r1 X_{h2} + 2 r2 X_{h2}} Q\, r1 + e^{L r1 + L r2 + r1 X_h + r2 X_h + r1 X_{h1} + r1 X_{h2} + r2 X_{h2}} Q1\, r1 -$$
$$e^{L r1 + L r2 + r1 X_h + r1 X_{h1} + r2 X_{h1} + r1 X_{h2} + r2 X_{h2}} Q1\, r1 + e^{L r1 + L r2 + r1 X_h + 2 r2 X_h + r1 X_{h1} + r2 X_{h1} + r1 X_{h2} + r2 X_{h2}} Q1\, r1 -$$
$$e^{L r1 + L r2 + r1 X_h + r2 X_h + r1 X_{h1} + 2 r2 X_{h1} + r1 X_{h2} + r2 X_{h2}} Q1\, r1 + e^{2 L r1 + r1 X_h + r2 X_h + r1 X_{h1} + r2 X_{h1} + r2 X_{h2}} Q\, r2 -$$
$$e^{2 L r1 + r1 X_h + r2 X_h + r1 X_{h1} + r2 X_{h1} + 2 r1 X_{h2} + r2 X_{h2}} Q\, r2 - e^{2 L r1 + r1 X_h + r2 X_h + r2 X_{h1} + r1 X_{h2} + r2 X_{h2}} Q1\, r2 +$$
$$e^{2 L r1 + r2 X_h + r1 X_{h1} + r2 X_{h1} + r1 X_{h2} + r2 X_{h2}} Q1\, r2 - e^{2 L r1 + 2 r1 X_h + r2 X_h + r1 X_{h1} + r2 X_{h1} + r1 X_{h2} + r2 X_{h2}} Q1\, r2 +$$
$$e^{2 L r1 + r1 X_h + r2 X_h + 2 r1 X_{h1} + r2 X_{h1} + r1 X_{h2} + r2 X_{h2}} Q1\, r2\Big),$$

$$B_1 \to -\frac{1}{\left(-e^{2 L r1} + e^{2 L r2}\right) G \left(-r1 + r2\right)} e^{-r1 X_h - r2 X_h - r1 X_{h1} - r2 X_{h1} - r1 X_{h2} - r2 X_{h2}}$$
$$\Big(-e^{2 L r2 + r1 X_h + r2 X_h + r1 X_{h1} + r2 X_{h1} + r1 X_{h2}} Q\, r1 + e^{2 L r2 + r1 X_h + r2 X_h + r1 X_{h1} + r2 X_{h1} + r1 X_{h2} + 2 r2 X_{h2}} Q\, r1 +$$
$$e^{2 L r2 + r1 X_h + r2 X_h + r1 X_{h1} + r1 X_{h2} + r2 X_{h2}} Q1\, r1 - e^{2 L r2 + r1 X_h + r1 X_{h1} + r2 X_{h1} + r1 X_{h2} + r2 X_{h2}} Q1\, r1 +$$
$$e^{2 L r2 + r1 X_h + 2 r2 X_h + r1 X_{h1} + r2 X_{h1} + r1 X_{h2} + r2 X_{h2}} Q1\, r1 - e^{2 L r2 + r1 X_h + r2 X_h + r1 X_{h1} + 2 r2 X_{h1} + r1 X_{h2} + r2 X_{h2}} Q1\, r1 +$$
$$e^{L r1 + L r2 + r1 X_h + r2 X_h + r1 X_{h1} + r2 X_{h1} + r2 X_{h2}} Q\, r2 - e^{L r1 + L r2 + r1 X_h + r2 X_h + r1 X_{h1} + r2 X_{h1} + 2 r1 X_{h2} + r2 X_{h2}} Q\, r2 -$$
$$e^{L r1 + L r2 + r1 X_h + r2 X_h + r2 X_{h1} + r1 X_{h2} + r2 X_{h2}} Q1\, r2 + e^{L r1 + L r2 + r2 X_h + r1 X_{h1} + r2 X_{h1} + r1 X_{h2} + r2 X_{h2}} Q1\, r2 -$$
$$e^{L r1 + L r2 + 2 r1 X_h + r2 X_h + r1 X_{h1} + r2 X_{h1} + r1 X_{h2} + r2 X_{h2}} Q1\, r2 +$$
$$e^{L r1 + L r2 + r1 X_h + r2 X_h + 2 r1 X_{h1} + r2 X_{h1} + r1 X_{h2} + r2 X_{h2}} Q1\, r2\Big),$$

$$A_2 \to -\frac{1}{\left(-e^{2 L r1} + e^{2 L r2}\right) G \left(r1 - r2\right)} e^{-r1 X_h - r2 X_h - r1 X_{h1} - r2 X_{h1} - r1 X_{h2} - r2 X_{h2}}$$
$$\Big(-e^{L r1 + L r2 + r1 X_h + r2 X_h + r1 X_{h1} + r2 X_{h1} + r1 X_{h2}} Q\, r1 + e^{L r1 + L r2 + r1 X_h + r2 X_h + r1 X_{h1} + r2 X_{h1} + r1 X_{h2} + 2 r2 X_{h2}} Q\, r1 +$$
$$e^{L r1 + L r2 + r1 X_h + r2 X_h + r1 X_{h1} + r1 X_{h2} + r2 X_{h2}} Q1\, r1 - e^{L r1 + L r2 + r1 X_h + r1 X_{h1} + r2 X_{h1} + r1 X_{h2} + r2 X_{h2}} Q1\, r1 +$$
$$e^{L r1 + L r2 + r1 X_h + 2 r2 X_h + r1 X_{h1} + r2 X_{h1} + r1 X_{h2} + r2 X_{h2}} Q1\, r1 - e^{L r1 + L r2 + r1 X_h + r2 X_h + r1 X_{h1} + 2 r2 X_{h1} + r1 X_{h2} + r2 X_{h2}}$$
$$Q1\, r1 + e^{2 L r1 + r1 X_h + r2 X_h + r1 X_{h1} + r2 X_{h1} + r2 X_{h2}} Q\, r2 - e^{2 L r1 + r1 X_h + r2 X_h + r1 X_{h1} + r2 X_{h1} + 2 r1 X_{h2} + r2 X_{h2}} Q\, r2 -$$
$$e^{2 L r1 + r1 X_h + r2 X_h + r2 X_{h1} + r1 X_{h2} + r2 X_{h2}} Q1\, r2 + e^{2 L r1 + r2 X_h + r1 X_{h1} + r2 X_{h1} + r1 X_{h2} + r2 X_{h2}} Q1\, r2 -$$
$$e^{2 L r2 + 2 r1 X_h + r2 X_h + r1 X_{h1} + r2 X_{h1} + r1 X_{h2} + r2 X_{h2}} Q1\, r2 + e^{2 L r2 + r1 X_h + r2 X_h + 2 r1 X_{h1} + r2 X_{h1} + r1 X_{h2} + r2 X_{h2}} Q1\, r2\Big),$$

$$B_2 \to -\frac{1}{\left(e^{2 L r1} - e^{2 L r2}\right) G \left(r1 - r2\right)} e^{-r1 X_h - r2 X_h - r1 X_{h1} - r2 X_{h1} - r1 X_{h2} - r2 X_{h2}}$$
$$\Big(-e^{2 L r2 + r1 X_h + r2 X_h + r1 X_{h1} + r2 X_{h1} + r1 X_{h2}} Q\, r1 + e^{2 L r2 + r1 X_h + r2 X_h + r1 X_{h1} + r2 X_{h1} + r1 X_{h2} + 2 r2 X_{h2}} Q\, r1 +$$
$$e^{2 L r2 + r1 X_h + r2 X_h + r1 X_{h1} + r1 X_{h2} + r2 X_{h2}} Q1\, r1 - e^{2 L r2 + r1 X_h + r1 X_{h1} + r2 X_{h1} + r1 X_{h2} + r2 X_{h2}} Q1\, r1 +$$
$$e^{2 L r1 + r1 X_h + 2 r2 X_h + r1 X_{h1} + r2 X_{h1} + r1 X_{h2} + r2 X_{h2}} Q1\, r1 - e^{2 L r1 + r1 X_h + r2 X_h + r1 X_{h1} + 2 r2 X_{h1} + r1 X_{h2} + r2 X_{h2}} Q1\, r1 +$$
$$e^{L r1 + L r2 + r1 X_h + r2 X_h + r1 X_{h1} + r2 X_{h1} + r2 X_{h2}} Q\, r2 - e^{L r1 + L r2 + r1 X_h + r2 X_h + r1 X_{h1} + r2 X_{h1} + 2 r1 X_{h2} + r2 X_{h2}} Q\, r2 -$$

$$e^{L\, r1+L\, r2+r1\, X_h+r2\, X_h+r2\, X_{h1}+r1\, X_{h2}+r2\, X_{h2}}\, Q1\, r2+e^{L\, r1+L\, r2+r2\, X_h+r1\, X_{h1}+r2\, X_{h1}+r1\, X_{h2}+r2\, X_{h2}}\, Q1\, r2-$$
$$e^{L\, r1+L\, r2+2\, r1\, X_h+r2\, X_h+r1\, X_{h1}+r2\, X_{h1}+r1\, X_{h2}+r2\, X_{h2}}\, Q1\, r2+$$
$$e^{L\, r1+L\, r2+r1\, X_h+r2\, X_h+2\, r1\, X_{h1}+r2\, X_{h1}+r1\, X_{h2}+r2\, X_{h2}}\, Q1\, r2\Big),$$

$$A_3\to-\frac{1}{\left(-e^{2\, L\, r1}+e^{2\, L\, r2}\right)\, G\, (r1-r2)}\, e^{-r1\, X_h-r2\, X_h-r1\, X_{h1}-r2\, X_{h1}-r1\, X_{h2}-r2\, X_{h2}}$$
$$\Big(-e^{L\, r1+L\, r2+r1\, X_h+r2\, X_h+r1\, X_{h1}+r2\, X_{h1}+r1\, X_{h2}}\, Q\, r1+e^{L\, r1+L\, r2+r1\, X_h+r2\, X_h+r1\, X_{h1}+r2\, X_{h1}+r1\, X_{h2}+2\, r2\, X_{h2}}\, Q\, r1+$$
$$e^{L\, r1+L\, r2+r1\, X_h+r2\, X_h+r1\, X_{h1}+r1\, X_{h2}+r2\, X_{h2}}\, Q1\, r1-e^{L\, r1+L\, r2+r1\, X_h+r1\, X_{h1}+r2\, X_{h1}+r1\, X_{h2}+r2\, X_{h2}}\, Q1\, r1+$$
$$e^{L\, r1+L\, r2+r1\, X_h+2\, r2\, X_h+r1\, X_{h1}+r2\, X_{h1}+r1\, X_{h2}+r2\, X_{h2}}\, Q1\, r1-e^{L\, r1+L\, r2+r1\, X_h+r2\, X_h+r1\, X_{h1}+2\, r2\, X_{h1}+r1\, X_{h2}+r2\, X_{h2}}$$
$$Q1\, r1+e^{2\, L\, r2+r1\, X_h+r2\, X_h+r1\, X_{h1}+r2\, X_{h1}+r2\, X_{h2}}\, Q\, r2-e^{2\, L\, r2+r1\, X_h+r2\, X_h+r1\, X_{h1}+r2\, X_{h1}+2\, r1\, X_{h2}+r2\, X_{h2}}\, Q\, r2-$$
$$e^{2\, L\, r1+r1\, X_h+r2\, X_h+r2\, X_{h1}+r1\, X_{h2}+r2\, X_{h2}}\, Q1\, r2+e^{2\, L\, r1+r2\, X_h+r1\, X_{h1}+r2\, X_{h1}+r1\, X_{h2}+r2\, X_{h2}}\, Q1\, r2-$$
$$e^{2\, L\, r2+2\, r1\, X_h+r2\, X_h+r1\, X_{h1}+r2\, X_{h1}+r1\, X_{h2}+r2\, X_{h2}}\, Q1\, r2+e^{2\, L\, r2+r1\, X_h+r2\, X_h+2\, r1\, X_{h1}+r2\, X_{h1}+r1\, X_{h2}+r2\, X_{h2}}\, Q1\, r2\Big),$$

$$B_3\to-\frac{1}{\left(e^{2\, L\, r1}-e^{2\, L\, r2}\right)\, G\, (-r1+r2)}\, e^{-r1\, X_h-r2\, X_h-r1\, X_{h1}-r2\, X_{h1}-r1\, X_{h2}-r2\, X_{h2}}$$
$$\Big(e^{2\, L\, r1+r1\, X_h+r2\, X_h+r1\, X_{h1}+r2\, X_{h1}+r1\, X_{h2}}\, Q\, r1-e^{2\, L\, r1+r1\, X_h+r2\, X_h+r1\, X_{h1}+r2\, X_{h1}+r1\, X_{h2}+2\, r2\, X_{h2}}\, Q\, r1-$$
$$e^{2\, L\, r2+r1\, X_h+r2\, X_h+r1\, X_{h1}+r1\, X_{h2}+r2\, X_{h2}}\, Q1\, r1+e^{2\, L\, r2+r1\, X_h+r1\, X_{h1}+r2\, X_{h1}+r1\, X_{h2}+r2\, X_{h2}}\, Q1\, r1-$$
$$e^{2\, L\, r1+r1\, X_h+2\, r2\, X_h+r1\, X_{h1}+r2\, X_{h1}+r1\, X_{h2}+r2\, X_{h2}}\, Q1\, r1+e^{2\, L\, r1+r1\, X_h+r2\, X_h+r1\, X_{h1}+2\, r2\, X_{h1}+r1\, X_{h2}+r2\, X_{h2}}\, Q1\, r1-$$
$$e^{L\, r1+L\, r2+r1\, X_h+r2\, X_h+r1\, X_{h1}+r2\, X_{h1}+r2\, X_{h2}}\, Q\, r2+e^{L\, r1+L\, r2+r1\, X_h+r2\, X_h+r1\, X_{h1}+r2\, X_{h1}+2\, r1\, X_{h2}+r2\, X_{h2}}\, Q\, r2+$$
$$e^{L\, r1+L\, r2+r1\, X_h+r2\, X_h+r2\, X_{h1}+r1\, X_{h2}+r2\, X_{h2}}\, Q1\, r2-e^{L\, r1+L\, r2+r2\, X_h+r1\, X_{h1}+r2\, X_{h1}+r1\, X_{h2}+r2\, X_{h2}}\, Q1\, r2+$$
$$e^{L\, r1+L\, r2+2\, r1\, X_h+r2\, X_h+r1\, X_{h1}+r2\, X_{h1}+r1\, X_{h2}+r2\, X_{h2}}\, Q1\, r2-$$
$$e^{L\, r1+L\, r2+r1\, X_h+r2\, X_h+2\, r1\, X_{h1}+r2\, X_{h1}+r1\, X_{h2}+r2\, X_{h2}}\, Q1\, r2\Big),$$

$$A_4\to-\frac{1}{\left(-e^{2\, L\, r1}+e^{2\, L\, r2}\right)\, G\, (r1-r2)}\, e^{L\, r2-r1\, X_h-r2\, X_h-r1\, X_{h1}-r2\, X_{h1}-r1\, X_{h2}-r2\, X_{h2}}$$
$$\Big(-e^{L\, r1+r1\, X_h+r2\, X_h+r1\, X_{h1}+r2\, X_{h1}+r1\, X_{h2}}\, Q\, r1+e^{L\, r1+r1\, X_h+r2\, X_h+r1\, X_{h1}+r2\, X_{h1}+r1\, X_{h2}+2\, r2\, X_{h2}}\, Q\, r1+$$
$$e^{L\, r1+r1\, X_h+r2\, X_h+r1\, X_{h1}+r1\, X_{h2}+r2\, X_{h2}}\, Q1\, r1-e^{L\, r1+r1\, X_h+r1\, X_{h1}+r2\, X_{h1}+r1\, X_{h2}+r2\, X_{h2}}\, Q1\, r1+$$
$$e^{L\, r1+r1\, X_h+2\, r2\, X_h+r1\, X_{h1}+r2\, X_{h1}+r1\, X_{h2}+r2\, X_{h2}}\, Q1\, r1-e^{L\, r1+r1\, X_h+r2\, X_h+r1\, X_{h1}+2\, r2\, X_{h1}+r1\, X_{h2}+r2\, X_{h2}}\, Q1\, r1+$$
$$e^{L\, r2+r1\, X_h+r2\, X_h+r1\, X_{h1}+r2\, X_{h1}+r2\, X_{h2}}\, Q\, r2-e^{L\, r2+r1\, X_h+r2\, X_h+r1\, X_{h1}+r2\, X_{h1}+2\, r1\, X_{h2}+r2\, X_{h2}}\, Q\, r2-$$
$$e^{L\, r2+r1\, X_h+r2\, X_h+r2\, X_{h1}+r1\, X_{h2}+r2\, X_{h2}}\, Q1\, r2+e^{L\, r2+r2\, X_h+r1\, X_{h1}+r2\, X_{h1}+r1\, X_{h2}+r2\, X_{h2}}\, Q1\, r2-$$
$$e^{L\, r2+2\, r1\, X_h+r2\, X_h+r1\, X_{h1}+r2\, X_{h1}+r1\, X_{h2}+r2\, X_{h2}}\, Q1\, r2+e^{L\, r2+r1\, X_h+r2\, X_h+2\, r1\, X_{h1}+r2\, X_{h1}+r1\, X_{h2}+r2\, X_{h2}}\, Q1\, r2\Big),$$

$$B_4\to-\frac{1}{\left(-e^{2\, L\, r1}+e^{2\, L\, r2}\right)\, G\, (-r1+r2)}\, e^{-r1\, X_h-r2\, X_h-r1\, X_{h1}-r2\, X_{h1}-r1\, X_{h2}-r2\, X_{h2}}$$
$$\Big(-e^{2\, L\, r1+r1\, X_h+r2\, X_h+r1\, X_{h1}+r2\, X_{h1}+r1\, X_{h2}}\, Q\, r1+e^{2\, L\, r1+r1\, X_h+r2\, X_h+r1\, X_{h1}+r2\, X_{h1}+r1\, X_{h2}+2\, r2\, X_{h2}}\, Q\, r1+$$
$$e^{2\, L\, r1+r1\, X_h+r2\, X_h+r1\, X_{h1}+r1\, X_{h2}+r2\, X_{h2}}\, Q1\, r1-e^{2\, L\, r1+r1\, X_h+r1\, X_{h1}+r2\, X_{h1}+r1\, X_{h2}+r2\, X_{h2}}\, Q1\, r1+$$
$$e^{2\, L\, r1+r1\, X_h+2\, r2\, X_h+r1\, X_{h1}+r2\, X_{h1}+r1\, X_{h2}+r2\, X_{h2}}\, Q1\, r1-e^{2\, L\, r1+r1\, X_h+r2\, X_h+r1\, X_{h1}+2\, r2\, X_{h1}+r1\, X_{h2}+r2\, X_{h2}}\, Q1\, r1+$$
$$e^{L\, r1+L\, r2+r1\, X_h+r2\, X_h+r1\, X_{h1}+r2\, X_{h1}+r2\, X_{h2}}\, Q\, r2-e^{L\, r1+L\, r2+r1\, X_h+r2\, X_h+r1\, X_{h1}+r2\, X_{h1}+2\, r1\, X_{h2}+r2\, X_{h2}}\, Q\, r2-$$
$$e^{L\, r1+L\, r2+r1\, X_h+r2\, X_h+r2\, X_{h1}+r1\, X_{h2}+r2\, X_{h2}}\, Q1\, r2+e^{L\, r1+L\, r2+r2\, X_h+r1\, X_{h1}+r2\, X_{h1}+r1\, X_{h2}+r2\, X_{h2}}\, Q1\, r2-$$
$$e^{L\, r1+L\, r2+2\, r1\, X_h+r2\, X_h+r1\, X_{h1}+r2\, X_{h1}+r1\, X_{h2}+r2\, X_{h2}}\, Q1\, r2+$$
$$e^{L\, r1+L\, r2+r1\, X_h+r2\, X_h+2\, r1\, X_{h1}+r2\, X_{h1}+r1\, X_{h2}+r2\, X_{h2}}\, Q1\, r2\Big),$$

$$C_1\to-\frac{1}{\left(-e^{2\, L\, r1}+e^{2\, L\, r2}\right)\, G\, (r1-r2)}\, e^{-r1\, X_h-r2\, X_h-r1\, X_{h1}-r2\, X_{h1}-r1\, X_{h2}-r2\, X_{h2}}$$
$$\Big(-e^{L\, r1+L\, r2+r1\, X_h+r2\, X_h+r1\, X_{h1}+r2\, X_{h1}+r1\, X_{h2}}\, Q\, r1+e^{L\, r1+L\, r2+r1\, X_h+r2\, X_h+r1\, X_{h1}+r2\, X_{h1}+r1\, X_{h2}+2\, r2\, X_{h2}}\, Q\, r1+$$
$$e^{L\, r1+L\, r2+r1\, X_h+r2\, X_h+r1\, X_{h1}+r1\, X_{h2}+r2\, X_{h2}}\, Q1\, r1-e^{L\, r1+L\, r2+r1\, X_h+r1\, X_{h1}+r2\, X_{h1}+r1\, X_{h2}+r2\, X_{h2}}\, Q1\, r1+$$
$$e^{L\, r1+L\, r2+r1\, X_h+2\, r2\, X_h+r1\, X_{h1}+r2\, X_{h1}+r1\, X_{h2}+r2\, X_{h2}}\, Q1\, r1-e^{L\, r1+L\, r2+r1\, X_h+r2\, X_h+r1\, X_{h1}+2\, r2\, X_{h1}+r1\, X_{h2}+r2\, X_{h2}}$$
$$Q1\, r1+e^{2\, L\, r1+r1\, X_h+r2\, X_h+r1\, X_{h1}+r2\, X_{h1}+r2\, X_{h2}}\, Q\, r2-e^{2\, L\, r1+r1\, X_h+r2\, X_h+r1\, X_{h1}+r2\, X_{h1}+2\, r1\, X_{h2}+r2\, X_{h2}}\, Q\, r2-$$
$$e^{2\, L\, r1+r1\, X_h+r2\, X_h+r2\, X_{h1}+r1\, X_{h2}+r2\, X_{h2}}\, Q1\, r2+e^{2\, L\, r1+r2\, X_h+r1\, X_{h1}+r2\, X_{h1}+r1\, X_{h2}+r2\, X_{h2}}\, Q1\, r2-$$
$$e^{2\, L\, r2+2\, r1\, X_h+r2\, X_h+r1\, X_{h1}+r2\, X_{h1}+r1\, X_{h2}+r2\, X_{h2}}\, Q1\, r2+e^{2\, L\, r1+r1\, X_h+r2\, X_h+2\, r1\, X_{h1}+r2\, X_{h1}+r1\, X_{h2}+r2\, X_{h2}}\, Q1\, r2\Big),$$

$$C_2\to-\frac{1}{\left(-e^{2\, L\, r1}+e^{2\, L\, r2}\right)\, G\, (-r1+r2)}\, e^{-r1\, X_h-r2\, X_h-r1\, X_{h1}-r2\, X_{h1}-r1\, X_{h2}-r2\, X_{h2}}$$
$$\Big(-e^{2\, L\, r2+r1\, X_h+r2\, X_h+r1\, X_{h1}+r2\, X_{h1}+r1\, X_{h2}}\, Q\, r1+e^{2\, L\, r2+r1\, X_h+r2\, X_h+r1\, X_{h1}+r2\, X_{h1}+r1\, X_{h2}+2\, r2\, X_{h2}}\, Q\, r1+$$
$$e^{2\, L\, r2+r1\, X_h+r2\, X_h+r1\, X_{h1}+r1\, X_{h2}+r2\, X_{h2}}\, Q1\, r1-e^{2\, L\, r2+r1\, X_h+r1\, X_{h1}+r2\, X_{h1}+r1\, X_{h2}+r2\, X_{h2}}\, Q1\, r1+$$
$$e^{2\, L\, r1+r1\, X_h+2\, r2\, X_h+r1\, X_{h1}+r2\, X_{h1}+r1\, X_{h2}+r2\, X_{h2}}\, Q1\, r1-e^{2\, L\, r2+r1\, X_h+r2\, X_h+r1\, X_{h1}+2\, r2\, X_{h1}+r1\, X_{h2}+r2\, X_{h2}}\, Q1\, r1+$$
$$e^{L\, r1+L\, r2+r1\, X_h+r2\, X_h+r1\, X_{h1}+r2\, X_{h1}+r2\, X_{h2}}\, Q\, r2-e^{L\, r1+L\, r2+r1\, X_h+r2\, X_h+r1\, X_{h1}+r2\, X_{h1}+2\, r1\, X_{h2}+r2\, X_{h2}}\, Q\, r2-$$

$$
\begin{aligned}
&e^{L\,r1+L\,r2+r1\,X_h+r2\,X_h+r2\,X_{h1}+r1\,X_{h2}+r2\,X_{h2}}\,Q1\,r2+e^{L\,r1+L\,r2+r2\,X_h+r1\,X_{h1}+r2\,X_{h1}+r1\,X_{h2}+r2\,X_{h2}}\,Q1\,r2-\\
&e^{L\,r1+L\,r2+2\,r1\,X_h+r2\,X_h+r1\,X_{h1}+r2\,X_{h1}+r1\,X_{h2}+r2\,X_{h2}}\,Q1\,r2+\\
&e^{L\,r1+L\,r2+r1\,X_h+r2\,X_h+2\,r1\,X_{h1}+r2\,X_{h1}+r1\,X_{h2}+r2\,X_{h2}}\,Q1\,r2\Big),
\end{aligned}
$$

$$
\begin{aligned}
C_3\to&-\frac{1}{\left(-e^{2\,L\,r1}+e^{2\,L\,r2}\right)\,G\,\left(r1-r2\right)}\,e^{-r1\,X_h-r2\,X_h-r1\,X_{h1}-r2\,X_{h1}-r1\,X_{h2}-r2\,X_{h2}}\\
&\Big(-e^{L\,r1+L\,r2+r1\,X_h+r2\,X_h+r1\,X_{h1}+r2\,X_{h1}+r1\,X_{h2}}\,Q\,r1+e^{L\,r1+L\,r2+r1\,X_h+r2\,X_h+r1\,X_{h1}+r2\,X_{h1}+r1\,X_{h2}+2\,r2\,X_{h2}}\,Q\,r1+\\
&e^{L\,r1+L\,r2+r1\,X_h+r2\,X_h+r1\,X_{h1}+r1\,X_{h2}+r2\,X_{h2}}\,Q1\,r1-e^{L\,r1+L\,r2+r1\,X_h+r1\,X_{h1}+r2\,X_{h1}+r1\,X_{h2}+r2\,X_{h2}}\,Q1\,r1+\\
&e^{L\,r1+L\,r2+r1\,X_h+2\,r2\,X_h+r1\,X_{h1}+r2\,X_{h1}+r1\,X_{h2}+r2\,X_{h2}}\,Q1\,r1-e^{L\,r1+L\,r2+r1\,X_h+r2\,X_h+r1\,X_{h1}+2\,r2\,X_{h1}+r1\,X_{h2}+r2\,X_{h2}}\\
&Q1\,r1+e^{2\,L\,r1+r1\,X_h+r2\,X_h+r1\,X_{h1}+r2\,X_{h1}+r2\,X_{h2}}\,Q\,r2-e^{2\,L\,r2+r1\,X_h+r2\,X_h+r1\,X_{h1}+r2\,X_{h1}+2\,r1\,X_{h2}+r2\,X_{h2}}\,Q\,r2-\\
&e^{2\,L\,r1+r1\,X_h+r2\,X_h+r2\,X_{h1}+r1\,X_{h2}+r2\,X_{h2}}\,Q1\,r2+e^{2\,L\,r1+r2\,X_h+r1\,X_{h1}+r2\,X_{h1}+r1\,X_{h2}+r2\,X_{h2}}\,Q1\,r2-\\
&e^{2\,L\,r2+2\,r1\,X_h+r2\,X_h+r1\,X_{h1}+r2\,X_{h1}+r1\,X_{h2}+r2\,X_{h2}}\,Q1\,r2+e^{2\,L\,r2+r1\,X_h+r2\,X_h+2\,r1\,X_{h1}+r2\,X_{h1}+r1\,X_{h2}+r2\,X_{h2}}\,Q1\,r2\Big),
\end{aligned}
$$

$$
\begin{aligned}
C_4\to&-\frac{1}{\left(e^{2\,L\,r1}-e^{2\,L\,r2}\right)\,G\,\left(r1-r2\right)}\,e^{-r1\,X_h-r2\,X_h-r1\,X_{h1}-r2\,X_{h1}-r1\,X_{h2}-r2\,X_{h2}}\\
&\Big(-e^{2\,L\,r2+r1\,X_h+r2\,X_h+r1\,X_{h1}+r2\,X_{h1}+r1\,X_{h2}}\,Q\,r1+e^{2\,L\,r1+r1\,X_h+r2\,X_h+r1\,X_{h1}+r2\,X_{h1}+r1\,X_{h2}+2\,r2\,X_{h2}}\,Q\,r1+\\
&e^{2\,L\,r2+r1\,X_h+r2\,X_h+r1\,X_{h1}+r1\,X_{h2}+r2\,X_{h2}}\,Q1\,r1-e^{2\,L\,r2+r1\,X_h+r1\,X_{h1}+r2\,X_{h1}+r1\,X_{h2}+r2\,X_{h2}}\,Q1\,r1+\\
&e^{2\,L\,r1+r1\,X_h+2\,r2\,X_h+r1\,X_{h1}+r2\,X_{h1}+r1\,X_{h2}+r2\,X_{h2}}\,Q1\,r1-e^{2\,L\,r1+r1\,X_h+r2\,X_h+r1\,X_{h1}+2\,r2\,X_{h1}+r1\,X_{h2}+r2\,X_{h2}}\,Q1\,r1+\\
&e^{L\,r1+L\,r2+r1\,X_h+r2\,X_h+r1\,X_{h1}+r2\,X_{h1}+r2\,X_{h2}}\,Q\,r2-e^{L\,r1+L\,r2+r1\,X_h+r2\,X_h+r1\,X_{h1}+r2\,X_{h1}+2\,r1\,X_{h2}+r2\,X_{h2}}\,Q\,r2-\\
&e^{L\,r1+L\,r2+r1\,X_h+r2\,X_h+r2\,X_{h1}+r1\,X_{h2}+r2\,X_{h2}}\,Q1\,r2+e^{L\,r1+L\,r2+r2\,X_h+r1\,X_{h1}+r2\,X_{h1}+r1\,X_{h2}+r2\,X_{h2}}\,Q1\,r2-\\
&e^{L\,r1+L\,r2+2\,r1\,X_h+r2\,X_h+r1\,X_{h1}+r2\,X_{h1}+r1\,X_{h2}+r2\,X_{h2}}\,Q1\,r2+\\
&e^{L\,r1+L\,r2+r1\,X_h+r2\,X_h+2\,r1\,X_{h1}+r2\,X_{h1}+r1\,X_{h2}+r2\,X_{h2}}\,Q1\,r2\Big),
\end{aligned}
$$

$$
\begin{aligned}
C_5\to&-\frac{1}{\left(-e^{2\,L\,r1}+e^{2\,L\,r2}\right)\,G\,\left(r1-r2\right)}\,e^{-r1\,X_h-r2\,X_h-r1\,X_{h1}-r2\,X_{h1}-r1\,X_{h2}-r2\,X_{h2}}\\
&\Big(-e^{L\,r1+L\,r2+r1\,X_h+r2\,X_h+r1\,X_{h1}+r2\,X_{h1}+r1\,X_{h2}}\,Q\,r1+e^{L\,r1+L\,r2+r1\,X_h+r2\,X_h+r1\,X_{h1}+r2\,X_{h1}+r1\,X_{h2}+2\,r2\,X_{h2}}\,Q\,r1+\\
&e^{L\,r1+L\,r2+r1\,X_h+r2\,X_h+r1\,X_{h1}+r1\,X_{h2}+r2\,X_{h2}}\,Q1\,r1-e^{L\,r1+L\,r2+r1\,X_h+r1\,X_{h1}+r2\,X_{h1}+r1\,X_{h2}+r2\,X_{h2}}\,Q1\,r1+\\
&e^{L\,r1+L\,r2+r1\,X_h+2\,r2\,X_h+r1\,X_{h1}+r2\,X_{h1}+r1\,X_{h2}+r2\,X_{h2}}\,Q1\,r1-e^{L\,r1+L\,r2+r1\,X_h+r2\,X_h+r1\,X_{h1}+2\,r2\,X_{h1}+r1\,X_{h2}+r2\,X_{h2}}\\
&Q1\,r1+e^{2\,L\,r2+r1\,X_h+r2\,X_h+r1\,X_{h1}+r2\,X_{h1}+r2\,X_{h2}}\,Q\,r2-e^{2\,L\,r2+r1\,X_h+r2\,X_h+r1\,X_{h1}+r2\,X_{h1}+2\,r1\,X_{h2}+r2\,X_{h2}}\,Q\,r2-\\
&e^{2\,L\,r2+r1\,X_h+r2\,X_h+r2\,X_{h1}+r1\,X_{h2}+r2\,X_{h2}}\,Q1\,r2+e^{2\,L\,r1+r2\,X_h+r1\,X_{h1}+r2\,X_{h1}+r1\,X_{h2}+r2\,X_{h2}}\,Q1\,r2-\\
&e^{2\,L\,r2+2\,r1\,X_h+r2\,X_h+r1\,X_{h1}+r2\,X_{h1}+r1\,X_{h2}+r2\,X_{h2}}\,Q1\,r2+e^{2\,L\,r2+r1\,X_h+r2\,X_h+2\,r1\,X_{h1}+r2\,X_{h1}+r1\,X_{h2}+r2\,X_{h2}}\,Q1\,r2\Big),
\end{aligned}
$$

$$
\begin{aligned}
C_6\to&-\frac{1}{\left(e^{2\,L\,r1}-e^{2\,L\,r2}\right)\,G\,\left(-r1+r2\right)}\,e^{-r1\,X_h-r2\,X_h-r1\,X_{h1}-r2\,X_{h1}-r1\,X_{h2}-r2\,X_{h2}}\\
&\Big(e^{2\,L\,r1+r1\,X_h+r2\,X_h+r1\,X_{h1}+r2\,X_{h1}+r1\,X_{h2}}\,Q\,r1-e^{2\,L\,r1+r1\,X_h+r2\,X_h+r1\,X_{h1}+r2\,X_{h1}+r1\,X_{h2}+2\,r2\,X_{h2}}\,Q\,r1-\\
&e^{2\,L\,r1+r1\,X_h+r2\,X_h+r1\,X_{h1}+r1\,X_{h2}+r2\,X_{h2}}\,Q1\,r1+e^{2\,L\,r2+r1\,X_h+r1\,X_{h1}+r2\,X_{h1}+r1\,X_{h2}+r2\,X_{h2}}\,Q1\,r1-\\
&e^{2\,L\,r1+r1\,X_h+2\,r2\,X_h+r1\,X_{h1}+r2\,X_{h1}+r1\,X_{h2}+r2\,X_{h2}}\,Q1\,r1+e^{2\,L\,r1+r1\,X_h+r2\,X_h+r1\,X_{h1}+2\,r2\,X_{h1}+r1\,X_{h2}+r2\,X_{h2}}\,Q1\,r1-\\
&e^{L\,r1+L\,r2+r1\,X_h+r2\,X_h+r1\,X_{h1}+r2\,X_{h1}+r2\,X_{h2}}\,Q\,r2+e^{L\,r1+L\,r2+r1\,X_h+r2\,X_h+r1\,X_{h1}+r2\,X_{h1}+2\,r1\,X_{h2}+r2\,X_{h2}}\,Q\,r2+\\
&e^{L\,r1+L\,r2+r1\,X_h+r2\,X_h+r2\,X_{h1}+r1\,X_{h2}+r2\,X_{h2}}\,Q1\,r2-e^{L\,r1+L\,r2+r2\,X_h+r1\,X_{h1}+r2\,X_{h1}+r1\,X_{h2}+r2\,X_{h2}}\,Q1\,r2+\\
&e^{L\,r1+L\,r2+2\,r1\,X_h+r2\,X_h+r1\,X_{h1}+r2\,X_{h1}+r1\,X_{h2}+r2\,X_{h2}}\,Q1\,r2-\\
&e^{L\,r1+L\,r2+r1\,X_h+r2\,X_h+2\,r1\,X_{h1}+r2\,X_{h1}+r1\,X_{h2}+r2\,X_{h2}}\,Q1\,r2\Big)\Big\}\Big\}
\end{aligned}
$$

Appendix D

The temperature profile of changing the distance between heaters

To understand how the distance between two heaters influences the sensitivity, we plot the temperature profile of different simulation in here. It can be seen from the figure as the distance between the two heaters increase, the temperature is dropped more, thus when we calculate the average temperature of two heaters, the value will be decreased and the temperature difference between two heaters will also be decreased. Then to reach a high sensitivity, the gap between the two heaters should as small as possible.

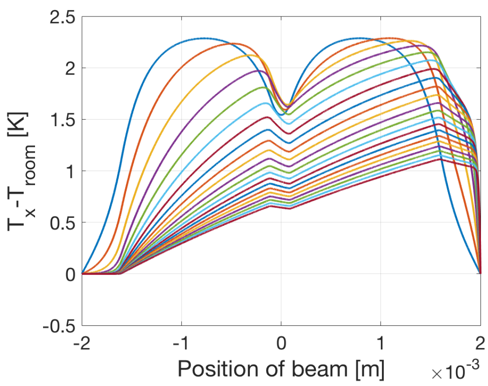

Figure D.1: The temperature profile of sensor with 1500 um heater and distance between two heaters is 200 um

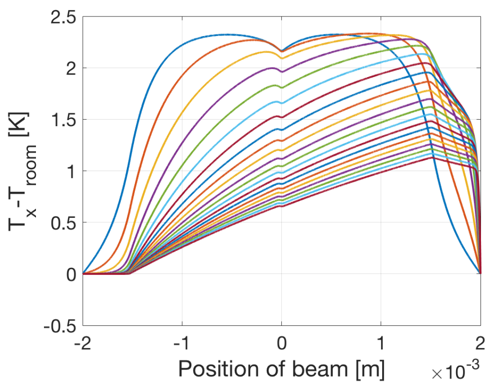

Figure D.2: The temperature profile of sensor with 1500 um heater and distance between two heaters is 40 um

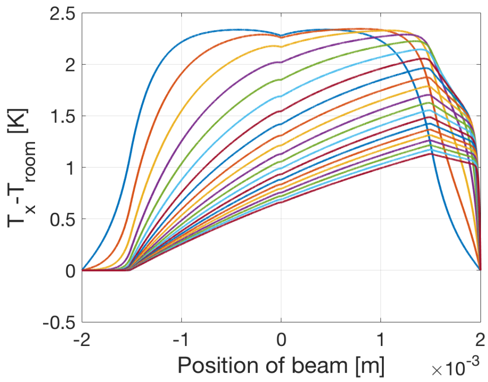

Figure D.3: The temperature profile of sensor with 1500 um heater and distance between two heaters is 16 um

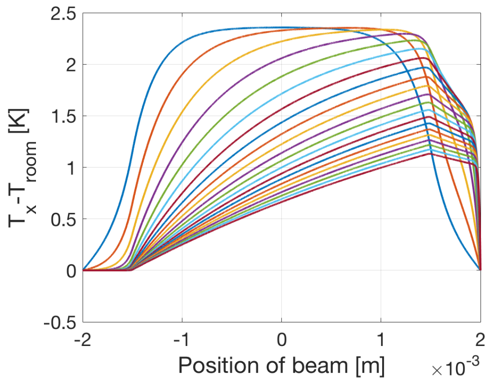

Figure D.4: The temperature profile of sensor with 1500 um heater and distance between two heaters is 0 um

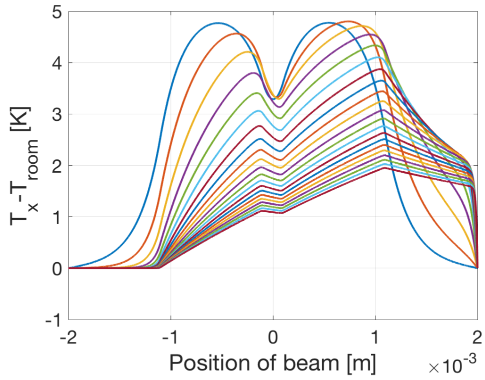

Figure D.5: The temperature profile of sensor with 1000 um heater and distance between two heaters is 200 um

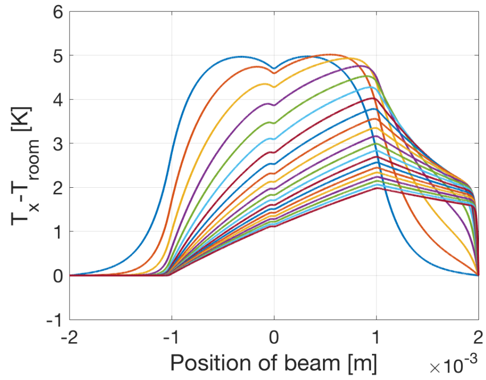

Figure D.6: The temperature profile of sensor with 1000 um heater and distance between two heaters is 40 um

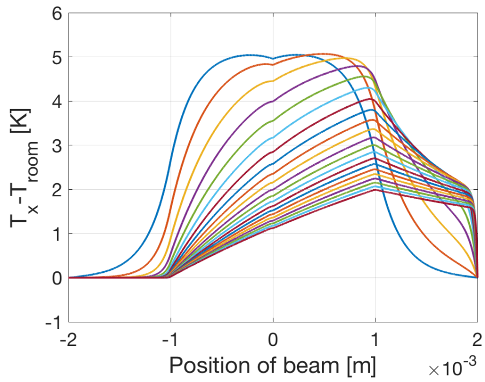

Figure D.7: The temperature profile of sensor with 1000 um heater and distance between two heaters is 16 um

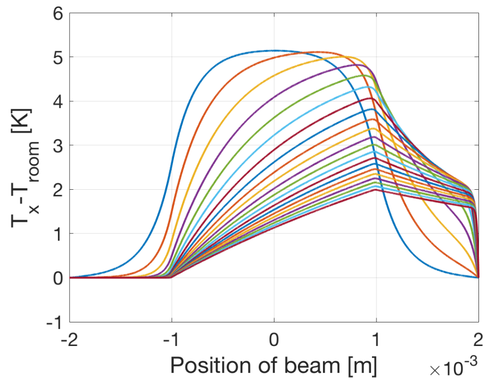

Figure D.8: The temperature profile of sensor with 1000 um heater and distance between two heaters is 0 um

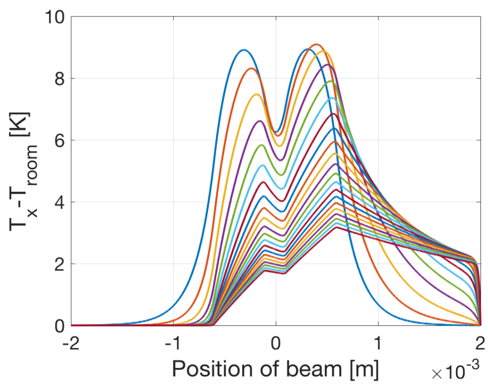

Figure D.9: The temperature profile of sensor with 500 um heater and distance between two heaters is 200 um

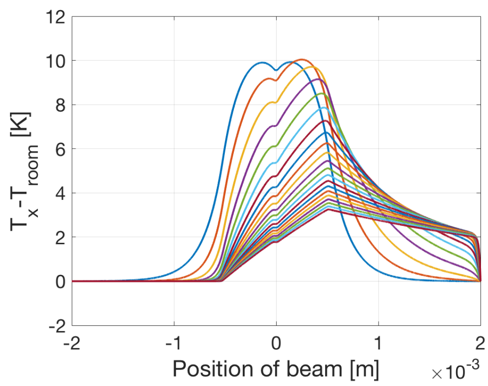

Figure D.10: The temperature profile of sensor with 500 um heater and distance between two heaters is 40 um

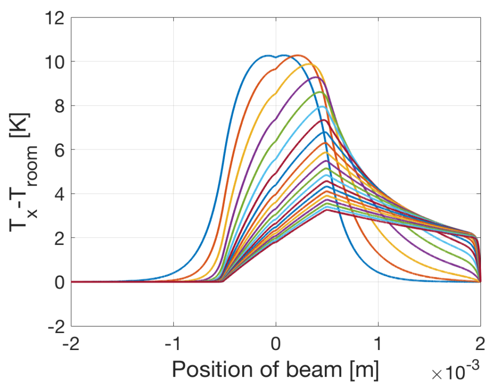

Figure D.11: The temperature profile of sensor with 500 um heater and distance between two heaters is 16 um

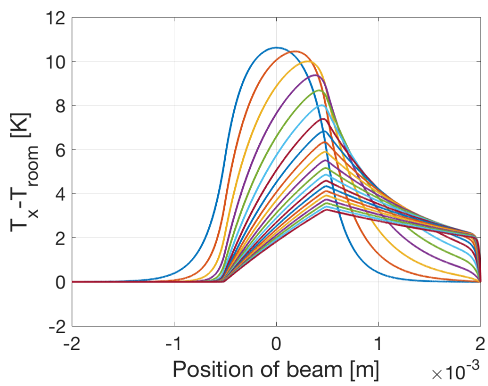

Figure D.12: The temperature profile of sensor with 500 um heater and distance between two heaters is 0 um

Appendix E

The temperature profile of changing the distance between heaters

In this section, the temperature profile of the sensor with different channel length will be presented. From the figure, it can be seen that when the channel length decreased, the heat-sink on the begging and end of the channel will force the temperature close to room temperature.

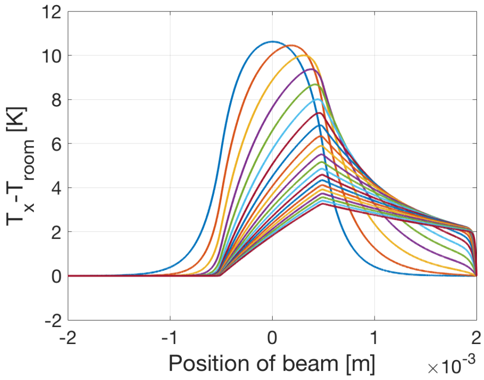

Figure E.1: The temperature profile of sensor with 500 um heater and channel length is 4000 um

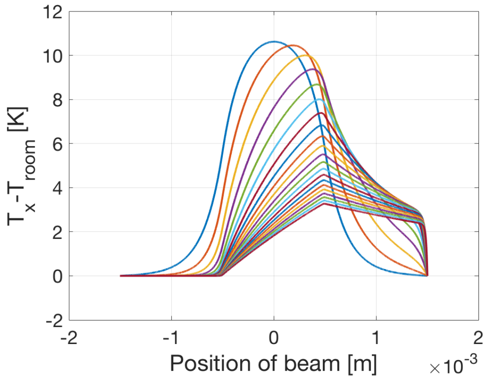

Figure E.2: The temperature profile of sensor with 500 um heater and channel length is 3000 um

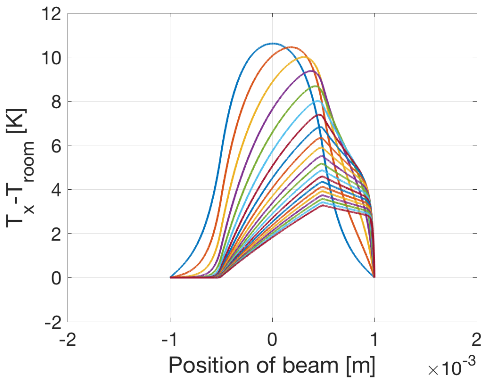

Figure E.3: The temperature profile of sensor with 500 um heater and channel length is 2000 um

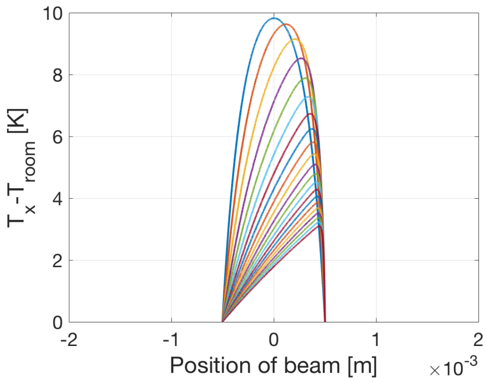

Figure E.4: The temperature profile of sensor with 500 um heater and channel length is 1000 um

Appendix F

New Thermal Flow Sensor

In this section, we will present the mask design for the new sensor, which is mentioned in the conclusion. The figure F.1 shows the mask of the new sensor, same as Bronkhorst sensor the sensor has asymmetric design and important structure are denoted as:

1. The channel with 31 um radius.
2. The channel with 55 um radius.
3. Pressure sensor.
4. Pressure sensor.
5. Inlet.
6. Outlet.
7. Temperature sensor.

Compare to the Bronkhorst sensor, the new sensor use only one heater in the middle and two measurement resistance placed on the side of heaters,see figure F.2. Because in chapter 3, we have investigated that if we want a high sensitivity sensor, the length of the heater and the gap between the two heaters should as shorter as possible, but if the heater is too short, the current will be limited, thus we need to make sure the short heater still can generate enough power. What is more, we integrated one temperature sensor in the chip, the temperature sensor will help us to measure the chip temperature, then we can calculate the temperature difference more accurate.

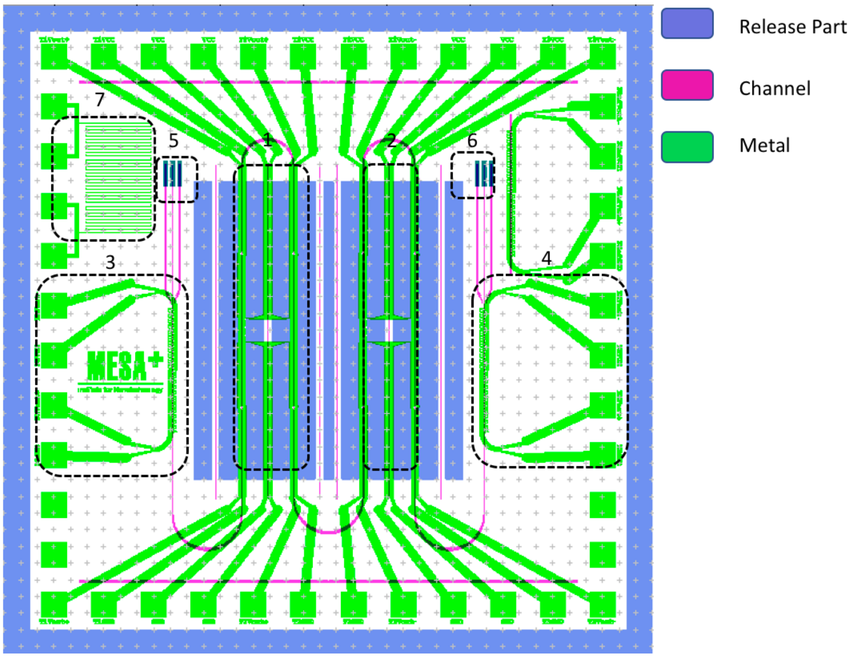

Figure F.1: The new thermal flow sensor, in design the dash bloc 6 is the temperature sensor to measuring the chip's temperature, the dash block 1 and 2 is the channel with 31.5 um and 55 um.

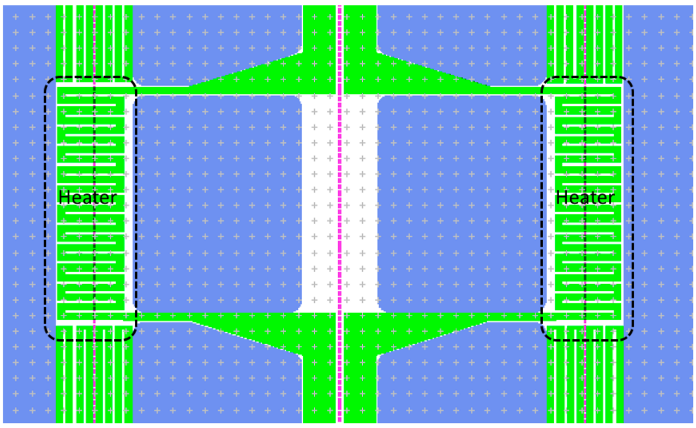

Figure F.2: There is only one heater in the middle of channel, on the two side is measurement resistance.